AGU PUBLICATIONS

JGR

Journal of Geophysical Research: Oceans

RESEARCH ARTICLE

10.1002/2017JC013518

Tropical Cyclone-Driven Sediment Dynamics Over the Australian North West Shelf

François Dufois[1,2,3], Ryan J. Lowe[1,2,3], Paul Branson[4], and Peter Fearns[5]

[1]The UWA Oceans Institute, University of Western Australia, Crawley, WA, Australia, [2]ARC Centre of Excellence for Coral Reef Studies, University of Western Australia, Crawley, WA, Australia, [3]School of Earth Sciences, University of Western Australia, Crawley, WA, Australia, [4]CSIRO Oceans and Atmosphere, Crawley, WA, Australia, [5]Remote Sensing and Satellite Research Group, Curtin University, Bentley, Perth, WA, Australia

Abstract Owing to their strong forcing at the air-sea interface, tropical cyclones are a major driver of hydrodynamics and sediment dynamics of continental shelves, strongly impacting marine habitats and offshore industries. Despite the North West Shelf of Australia being one of the most frequently impacted tropical cyclone regions worldwide, there is limited knowledge of how tropical cyclones influence the sediment dynamics of this shelf region, including the significance of these episodic extreme events to the normal background conditions that occur. Using an extensive 2 year data set of the in situ sediment dynamics and 14 yearlong calibrated satellite ocean-color data set, we demonstrate that alongshore propagating cyclones are responsible for simultaneously generating both strong wave-induced sediment resuspension events and significant southwestward subtidal currents. Over the 2 year study period, two particular cyclones (Iggy and Narelle) dominated the sediment fluxes resulting in a residual southwestward sediment transport over the southern part of the shelf. By analyzing results from a long-term (37 year) wind and wave hindcast, our results suggest that at least 16 tropical cyclones had a strong potential to contribute to that southwestward sediment pathway in a similar way to Iggy and Narelle.

Key Points:
- Over Australia's North West Shelf, tropical cyclones are the main drivers of suspended sediment dynamics
- Suspended sediment during cyclone events results from wave resuspension rather than advection of terrigenous material over most of the shelf
- The overall residual shelf sediment pathway is dominated by episodic tropical cyclone events generating southwestward wind-induced transport spanning the entire shelf

Supporting Information:
- Supporting Information S1

Correspondence to:
F. Dufois,
francois.dufois@uwa.edu.au

Citation:
Dufois, F., Lowe, R. J., Branson, P., & Fearns, P. (2017). Tropical cyclone-driven sediment dynamics over the Australian North West Shelf. *Journal of Geophysical Research: Oceans*, *122*, 10,225–10,244. https://doi.org/10.1002/2017JC013518

Received 29 SEP 2017
Accepted 2 DEC 2017
Accepted article online 11 DEC 2017
Published online 29 DEC 2017

1. Introduction

Australia's North West Shelf (NWS) is a rich continental margin both in terms of resources and biodiversity. Owing to its oil and gas production, and mineral export facilities, it is one of the most economically significant marine regions for Australia (Longley et al., 2002). The NWS and inshore coastal region also deliver significant ecosystem services to the region by hosting numerous high value marine ecosystems, including coral reefs, mangrove forests, and seagrass beds, that in turn support a wide range of fish communities and iconic fauna (e.g., dugongs, turtles, and whales; WAMSI, 2015; Wilson, 2013).

The NWS also has the highest occurrence of tropical cyclones (TCs) in the Indo-Pacific region, experiencing an average of ~3 TCs/yr between November and April (Condie et al., 2009; Hearn & Holloway, 1990; Lough, 1998). TCs can be a major driver of sediment dynamics of continental shelves worldwide (Dail et al., 2007; Galewsky et al., 2006; Larcombe & Carter, 2004; Liu et al., 2012), impacting benthic and pelagic habitats by changing water column turbidity (Madsen et al., 2001; Tian et al., 2009) or modifying seabed physical characteristics (Bridge et al., 2011; Sherman et al., 2016; Wolanski et al., 2008).

Over the NWS, TCs are known to substantially modify the offshore hydrodynamic conditions (Drost et al., 2017; Hearn & Holloway, 1990; Rayson et al., 2015) and induce flash flooding and intermittent coastal sediment discharge (Semeniuk, 1993), which together could be major drivers of the regional sediment dynamics. Sediment dynamics during TC events have also been suggested to be capable of modifying the light availability over the NWS that helps to dampen the phytoplankton bloom resulting from cyclone-driven nutrient enrichment (Condie et al., 2009). However, to date, detailed field observations of the NWS sediment dynamics under TCs are lacking in the literature, which are critical to fully quantify the importance of these sporadic extreme events relative to during typical "background" hydrodynamic conditions. Numerical modeling studies, although not validated with field observations, have nonetheless suggested that TCs are likely a major driver of sediment resuspension on the NWS (Harris, 1995; Harris et al., 2000; Porter-Smith et al., 2004) and can also drive substantial off-shelf sediment export (Condie et al., 2009).

Extensive marine developments, including dredging campaigns, have been taking place along the NWS during the last decade, to support the tremendous expansion of Australia's northwest resource industry (Fisher et al., 2015; Jones et al., 2015; WAMSI, 2015). In order to put these and other sources of anthropogenic sediment fluxes into the context of natural sources of sediment variability of the NWS, it is critical to better understand and predict the physical drivers of the regional sediment dynamics. In this study, we take advantage of an extensive data set of in situ sediment dynamics across the NWS and calibrated satellite ocean-color data to assess the impact of TCs relative to other physical drivers. We demonstrate that episodic tropical cyclones dominate the sediment dynamics over plurennial time scales.

2. Regional Setting

This study focuses on the NWS off the Pilbara coast, extending between the North West Cape to the Dampier Archipelago (Figure 1). The NWS extends up to 250 km offshore from an arid tropical coast before reaching the shelf break around 200 m depth. Prevailing winds are southwesterly on the southern part of the shelf and northwesterly on the northern part during the austral summer, shifting southeasterly along the entire shelf during winter (Condie et al., 2006).

The NWS circulation is influenced by the southwestward-flowing Holloway Current that partially supplies the poleward flowing eastern boundary Leeuwin Current during austral autumn and winter (D'Adamo et al., 2009; Holloway, 1995) that consolidates near the North West Cape (~22°S; Xu et al., 2015). During the remainder of the year, the southwesterly winds drive periodic reversals of this current over the shelf (Condie & Andrewartha, 2008; Ridgway & Godfrey, 2015). With an annual average transport of 1 Sv, the Holloway

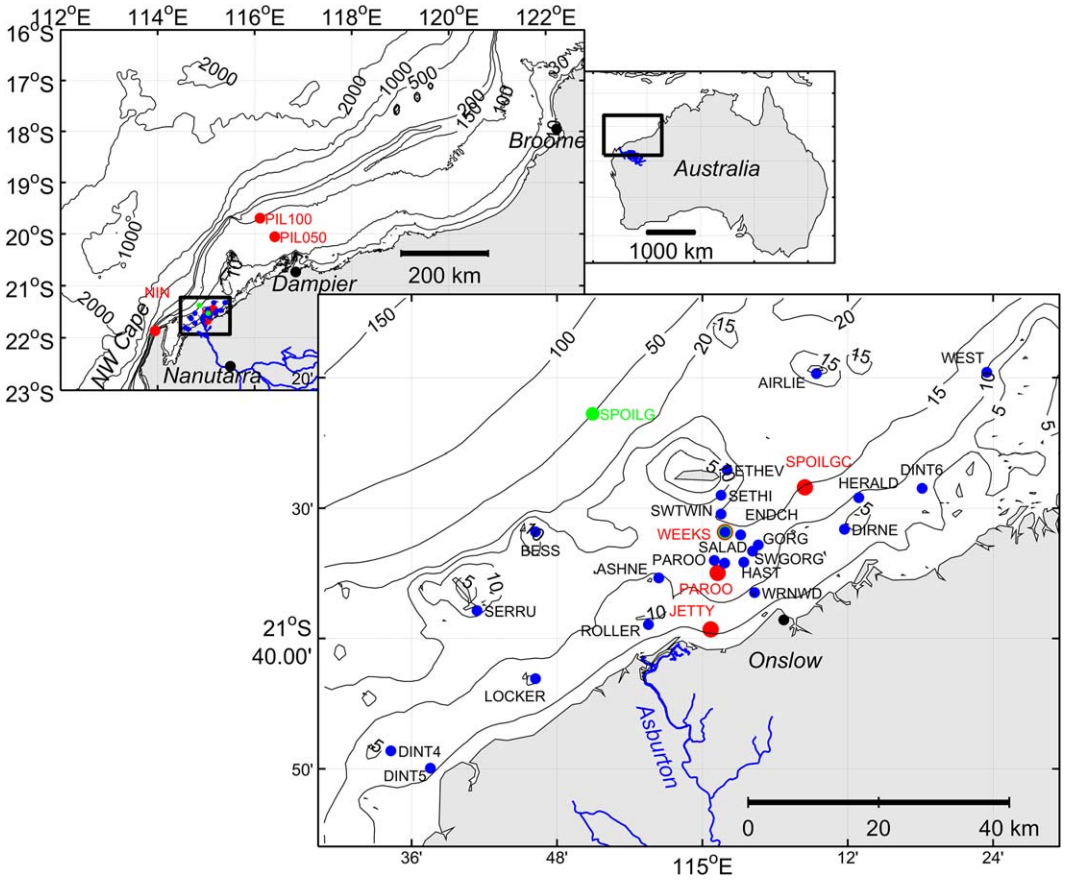

Figure 1. Study site, bathymetry, and location of the various sensors. Blue dots denote turbidity sensors and sediment traps, red dots represent current meters, and the green dots denote the wave buoy locations. The Ashburton River and its basin are indicated with blue lines on all maps. Isobaths are indicated with black lines.

Current peaks at ~2 Sv during winter/autumn, with current velocities reaching up to 0.2 m s^{-1} along the shelf break (Bahmanpour et al., 2016).

At daily time scales, the currents over the shelf are dominated by tidal motions. The semidiurnal tidal amplitudes and velocities vary strongly along the NWS, increasing northward. The tidal range can reach up to ~2 m near the North West Cape, ~4.5 m off Dampier, and ~9 m in Broome (Holloway, 1983). Peak tidal currents are predominantly in a cross-shore direction over the deeper parts of the shelf and are increasingly influenced by the bathymetry and the coastline orientation over the inner shelf (Condie et al., 2006; Holloway, 1983). The tidal currents often reach 1 m s^{-1} in the Pilbara region (~0.5 m s^{-1} off Onslow), and range 1–1.5 m s^{-1} further north (Condie et al., 2006; Porter-Smith et al., 2004). The combination of strong barotropic tides, density stratification, and steep topography also generate strong internal wave fields in areas deeper than ~100 m, with bottom currents reaching up to 1 m s^{-1} locally over the shelf (Rayson et al., 2011; Van Gastel et al., 2009).

The ocean response to TCs on the shelf circulation is complex, depending both on the cyclone characteristics and specific tracks (Fandry & Steedman, 1994; Hearn & Holloway, 1990; Rayson et al., 2015). Over the shelf, the response tends to be largely barotropic, and southwestward currents reaching 1 m s^{-1} can be generated between the coast and alongshore propagating cyclones (Fandry & Steedman, 1994; Hearn & Holloway, 1990). TCs can also trigger continental shelf waves propagating southward along the shelf, inducing water level and current velocity fluctuations with periods of several days (Eliot & Pattiaratchi, 2010; Webster, 1985). Cyclones also modify the stratification through enhanced mixing and can generate inertial motions and modulate the region's strong internal tides (Davidson & Holloway, 2003; Rayson et al., 2015).

During the austral winter months, wind wave energy over the shelf is predominantly related to remotely generated Southern Ocean storms, inducing long-period swell (>12 s) originating from the south-west (Hamilton, 1997). During summer, most of the high energy wave conditions are associated with tropical cyclones, with peak wave periods usually ranging between 8 and 12 s and with significant wave heights exceeding 10 m at the shelf break (Drost et al., 2017). Another dominant mode of wave energy during summer is associated with the diurnal sea-breeze cycle, generating short-period waves (<8 s; Hamilton, 1997). Overall, it is estimated that waves are higher than 3.5 m over the shelf between 10 and 30% of the time (Porter-Smith et al., 2004). However, the complex topography and the presence of islands, reefs, and shoals impact the wave propagation directions over the shelf, inducing inhomogeneous patterns of wave conditions at the shelf scale (Drost et al., 2017; Porter-Smith et al., 2004).

Seabed sediments across the NWS tend to be relatively coarse and composed primarily of sands and gravels, with a slight increase of the mud fraction along the shelf break and some nearshore areas (Jones, 1973). The sediments are considered mobile over most of the shelf in response to the local hydrodynamic environment (James et al., 2004; Jones, 1973; Porter-Smith et al., 2004). The sediment dynamics over the shelf are also influenced by the terrigenous sediment supply (Gingele et al., 2001). In the Pilbara region, the mean annual rainfall is only ~300 mm (Lough, 1998); however, extreme rainfall occurring during tropical cyclones and other tropical storms can induce flash flooding within the coastal zone, often providing most of the water and sediment river discharge in a given year (Semeniuk, 1993). The sediment load to the coastal zone is generally considered relatively low across the region, averaging ~0.3 Mt/yr (~10 kg s^{-1}) between the North West Cape and Dampier, with the Ashburton River being the main contributor, representing about half of the total solid discharge (Margvelashvili et al., 2006). The Ashburton catchment area is approximating 79,000 km^2 (Haig, 2009) and extends as far as ~600 km away from the river mouth (see Figure 1).

3. Methods

3.1. In Situ Field Observations

We compiled available in situ data from different sources for various locations across the Pilbara region, including data from wave buoys, acoustic current meters/profilers, turbidity sensors, and sediment traps, for the period spanning May 2011 to March 2013 (Table 1 and Figure 1). We used data from three current profilers from the Integrated Marine Observing System (IMOS) available at https://portal.aodn.org.au/(sensors Ningaloo, Pilbara 50 m, and Pilbara 100 m in Table 1 and Figure 1). All of the other in situ data were acquired as part of the Wheatstone project environmental management framework (Chevron, 2011, 2016)

Table 1
Location, Water Depth, and Instrument Types of the Various Sampling Sites, With Both the Site Name and the Site Code Used in the Text Included

Site name	Site code	Instrument	Site depth (m)	Sensor elevation	Longitude (°E)	Latitude (°S)
Current meter						
Ningaloo	NIN	RDI Workhorse 600 kHz	55	Bottom	113.947	21.867
Pilbara 50 m	PIL050	RDI Workhorse 300 kHz	47	Bottom	116.416	20.055
Pilbara 100 m	PIL100	RDI Workhorse 150 kHz	96	Bottom	116.112	19.694
Weeks shoal	WEEKS	Nortek Aquadopp 2 MHz	13.5	Bottom	115.031	21.529
Paroo shoal	PAROO	Nortek AWAC 1 MHz	10	Bottom	115.021	21.583
Jetty	JETTY	Nortek AWAC 1 MHz	8	Bottom	115.011	21.655
Spoil Ground C	SPOILGC	Nortek AWAC 1 MHz	15	Bottom	115.141	21.473
Wave buoy						
Spoil Ground	SPOILG	Datawell DWR MKIII	52	Surface	114.849	21.380
Weeks Shoal	WEEKS	Datawell DWR MKIII	13.5	Surface	115.031	21.529
Turbidity sensors and sediment traps						
Ward reef	WRNWD	WET Labs ECO	9	1.1 mab	115.072	21.608
Hastings shoal	HAST	WET Labs ECO	12	1.1 mab	115.057	21.569
Weeks shoal	WEEKS	WET Labs ECO	13	1.1 mab	115.031	21.529
Direction Island (NE)	DIRNE	WET Labs ECO	8	1.1 mab	115.196	21.527
Twin Island (SW)	SWTWIN	WET Labs ECO	8	1.1 mab	115.026	21.507
Gorgon patch	GORG	WET Labs ECO	12	1.1 mab	115.077	21.547
Gorgon patch (SW)	SWTWIN	WET Labs ECO	11	1.1 mab	115.069	21.555
Airlie Island	AIRLIE	WET Labs ECO	7	1.1 mab	115.157	21.328
Herald reef	HERALD	WET Labs ECO	8	1.1 mab	115.215	21.487
Thevenard Island (E)	ETHEV	WET Labs ECO	11	1.1 mab	115.034	21.451
Thevenard Island (SE)	SETHI	WET Labs ECO	9	1.1 mab	115.026	21.483
End of channel	ENDCH	WET Labs ECO	12	1.1 mab	115.053	21.534
Paroo shoal	PAROO	WET Labs ECO	11	1.1 mab	115.016	21.567
Saladin shoal	SALAD	WET Labs ECO	11	1.1 mab	115.031	21.570
Ashburton Island	ASHNE	WET Labs ECO	10	1.1 mab	114.940	21.589
Roller shoal	ROLLER	WET Labs ECO	10	1.1 mab	114.926	21.649
Bessiers Island	BESS	WET Labs ECO	8	1.1 mab	114.770	21.530
Serrurier Island	SERRU	WET Labs ECO	7	1.1 mab	114.690	21.631
West reef	WEST	WET Labs ECO	11	1.1 mab	115.391	21.326
Locker Island	LOCKER	WET Labs ECO	7	1.1 mab	114.770	21.718
Turbidity sensors						
Fly Island	DINT4	WET Labs ECO	11	1.1 mab	114.571	21.810
Tubridgi	DINT5	WET Labs ECO	7	1.1 mab	114.626	21.833
Mangrove	DINT6	WET Labs ECO	9	1.1 mab	115.302	21.475

Note. "mab" denotes meters above the bed.

and made available through the Western Australian Marine Science Institution (WAMSI) Joint Venture. This data set comprised data from 23 turbidity sensors, 20 sediment traps, 2 wave buoys, 3 current profilers, and 1 current meter deployed over a section of the shelf centered off Onslow. For a summary of all instrument sites and abbreviated site codes, refer to Table 1.

3.1.1. Wave and Currents

We used current measurements from four different locations over the inner shelf off Onslow (sites JETTY, PAROO, WEEKS, and SPOILGC in Figure 1) and from three deeper locations over a wider section of the shelf (sites NIN, PIL050, and PIL100). To isolate the subtidal flow variability, the tidal variations of the current velocity time series were filtered out using the Godin low-pass filter consisting of a succession of three running means with running windows of 24, 25, and 24 h (Godin, 1972).

We also used the significant wave height (H_s) and the mean period (T_m) from the wave buoys at site SPOILG, located at 52 m depth, offshore of most other inner shelf observations, and at site WEEKS, located at 13.5 m depth (Table 1 and Figure 1). We also used the wave parameters derived from Acoustic Surface Tracking (AST) from Nortek AWAC wave/current profilers at three locations (PAROO, JETTY, and SPOILGC).

3.1.2. Turbidity Measurements

The WET Labs ECO turbidity sensors were placed on fixed frames at 1.1 mab ("mab" denotes meters above the bed). The turbidity sensors were not calibrated to suspended sediment concentration (SSC) with in situ sediment, and therefore the turbidity is reported here in NTU. However, two relationships between turbidity and SSC were obtained posteriorly with a similar factory calibrated WET Labs ECO turbidity sensor to also provide a rough indication of the SSC concentrations:

$$\mathrm{SSC}\left[\mathrm{kg\ m^{-3}}\right] = a \times \mathrm{turbidity\ [NTU]} + b \tag{1}$$

The first calibration ($a = 1.07$, $b = 0.80$, $r = 0.99$, n = 42) was performed from in situ data from a 10 day field exercise sampling dredging plumes off Onslow (Fearns et al., 2017b). The second calibration ($a = 1.52$, $b = 2.25$, $r = 0.99$, n = 10) was derived from a tank experiment using seabed sediment collected in situ close to site ENDCH (Figure 1) and mechanically stirred uniformly through the water column (Fearns et al., 2017a).

We also estimated the turbidity profile throughout the water column by calibrating the backscatter data of the AWAC at PAROO using the nearest turbidity sensor (SALAD) located ~1.7 km away. Although those data provided useful insight into the water column sediment distribution, the results should be treated with caution (i.e., only qualitatively) considering the distance separating the AWAC and the turbidity sensor. We used the method detailed by Tessier et al. (2008) and adapted by Dufois et al. (2014) to estimate the turbidity from the AWAC in NTU. The echo intensity (*EI*, in counts) recorded by the AWAC was corrected for acoustic transmission losses, including spherical spreading and water absorption. With the turbidity at SALAD being lower than 100 NTU at any time, we neglected the sound attenuation induced by particles in suspension (Tessier, 2006). We therefore computed the relative volume backscattering strength (BS_r, in dB) for every bin of the AWAC following:

$$BS_r = K_c EI + 20\ \log_{10}\ (\psi R) + 2\alpha_w R \tag{2}$$

where K_c is a scaling factor taken as equal to 0.43 dB/count, α_w (in dB/m) is the coefficient of attenuation in water, ψ is the near-field correction of Downing et al. (1995) and R the distance from the transducer. We then computed the turbidity (in NTU) at every depth from BS_r following:

$$10\ \log_{10}\ (\mathrm{turbidity}) = aBS_r + b \tag{3}$$

where a and b were obtained by linear regression between the in situ turbidity and BS_r from the first AWAC bin located at 2 mab.

We also estimated the hourly cumulative turbidity flux vector at PAROO (using the turbidity from SALAD, i.e., from the turbidity instrument closest to PAROO) and at WEEKS following:

$$\vec{\Phi} = \left(\Phi_x, \Phi_y\right) = \sum_t \overrightarrow{U(t)} C(t) \Delta t \tag{4}$$

where $\overrightarrow{U(t)}$ and $C(t)$ are the velocity vector and the turbidity at time t, and Δt is the time step (1 h in this case).

3.1.3. Sediment Trap Data

The vertical sediment traps, made from PVC pipes with a diameter of 530 mm, were deployed near the turbidity sensors. At each sediment trap location, 11 deployments (referred to as P1–P11) were performed between December 2011 and March 2013. The sediment traps were recovered every 1–2 months at the time of mooring servicing. The total content captured by each trap was weighed to derive a total sedimentation rate. The inorganic sedimentation mass was also determined by loss on ignition at 550°C. The particle size distribution was analyzed using a laser diffraction particle size analyzer for diameters below 0.5 mm and wet sieving for greater diameters. Surficial sediment grabs were also taken at the deployment location at time of sediment trap recovery and analyzed for particle size distribution. We used the following grain size classification to present the data: clay (0–4 μm), silt (4–63 μm), very fine sand (63–125 μm), fine sand (125–250 μm), medium sand (250–500 μm), coarse sand (500–2000 μm), and gravel (>2,000 μm). We note that some sediment trap data were missing and all the parameters were not available for all the 11 deployment periods (e.g., all data for P7 and P8 were missing, and inorganic fraction data was missing for P9 and P10).

3.2. Additional Data Sources

We used the MODIS Aqua-derived and Terra-derived SSC products at 250 m resolution ranging June 2002 to December 2015 processed by Dorji et al. (2016) using a semianalytical model calibrated and validated specifically for the coastal waters within the same Pilbara study region. We composited the two products at the weekly time scale (at both 250 m and 4 km resolution) in order to have fewer gaps in the data set to allow for statistical processing. We acknowledge that the cloud cover could induce a negative bias on the weekly SSC composite by occluding the peak of the turbidity events especially during cyclone events. A comparison of in situ and satellite-based turbidity variability was therefore performed and is provided in section 4. In order to extract spatial and temporal patterns of SSC variability using satellite and in situ data, we used an Empirical Orthogonal Function (EOF) analysis (Legendre & Legendre, 2012).

The cyclone tracks, maximum winds, and cyclone radius (mean radius of the outermost closed isobar) were obtained from the Australian Bureau of Meteorology's historical tropical cyclone database (www.bom.gov.au). Wind data at the Onslow Airport were obtained from the Australian Bureau of Meteorology. We also extracted wind time series from the ECMWF ERA-Interim reanalysis for the period spanning 01/1979 to 12/2015 (Dee et al., 2011).

The Ashburton River daily discharge data were obtained from the Western Australian Department of Water (http://www.water.wa.gov.au). The closest river gauge is located at Nanutarra, about 120 km upstream of the Ashburton River mouth. We also extracted daily rainfall data from 18 stations homogeneously distributed over the Ashburton catchment area, available through the Australian Bureau of Meteorology.

To extend the in situ wave parameter time series for the period spanning 01/1979 to 12/2015 we used The Centre for Australian Weather and Climate Research (CAWCR) wave hindcast at 4′ (∼7 km) resolution based on the Wavewatch III model (Durrant et al., 2014; Hemer et al., 2016). We also computed the wave power per unit of wave crest (P) at SPOILG following: $P=EC_g$, where E is the wave mean energy, and C_g the wave group velocity determined using linear wave theory.

The wave and current-induced bottom shear stress (BSS) was computed following Dufois et al. (2014) assuming $z_0 = 0.3$ mm, which is a common value for seabeds composed of a mixture of mud, sand, and gravel consistent with the study area (Soulsby, 1997). The current-induced BSS was calculated using the bed-nearest velocity measurement and assuming a logarithmic velocity profile in the bottom boundary layer. The wave-induced BSS was derived from the near-bed orbital velocity calculated from H_s and T_m using linear wave theory.

4. Results

4.1. Tropical Cyclones and Meteorological Conditions

During the period spanning May 2011 to March 2013, there was the occurrence of six TCs where the track came within 1,000 km of Onslow (Figures 2 and 3a and supporting information Figure S1). TCs Iggy, Mitchell, and Narelle propagated alongshore over the ocean in a south-westward direction, passing Onslow approximately 400–500 km away offshore (Figure 2). Of these three TCs, Narelle was the strongest of all cyclones with wind reaching up to 54 m s^{-1} just off the Pilbara coast (Figures 2 and 3a). For Iggy, maximum winds were up to 31 m s^{-1}, reaching 28 m s^{-1} off the North West Cape. Mitchell winds peaked at 23 m s^{-1} off the North West Cape (Figure 2). In Onslow, Iggy and Narelle generated sustained (>10 m s^{-1}) easterly to northerly winds over several days, reaching up to 16 and 14 m s^{-1}, respectively (Figure 3b; detailed zoom results around the TCs are given in supporting information Figure S2). During Mitchell, sustained winds lasted for less than a day in Onslow where the strongest winds (reaching up to 12.5 m s^{-1}) were from a southeasterly direction.

TCs Heidi, Lua, and Rusty had more cross-shore trajectories within the Pilbara region and reached their strongest winds (41, 44, and 46 m s^{-1}, respectively) before making landfall between Broome and Dampier (Figures 2 and 3a and supporting information Figure S1). Lua originated ∼600 km offshore from Onslow. During this TC, the strongest winds locally in Onslow (reaching up to 14 m s^{-1}) were easterly to northeasterly and occurred when the cyclone was stationed ∼300 km offshore. Heidi and Rusty propagated eastward of Dampier. Southeasterly winds up to 12 m s^{-1} occurred in Onslow before Rusty made landfall. Heidi was the smallest cyclone with a radius of 296 km diameter at the maximum, compared to all other TC with

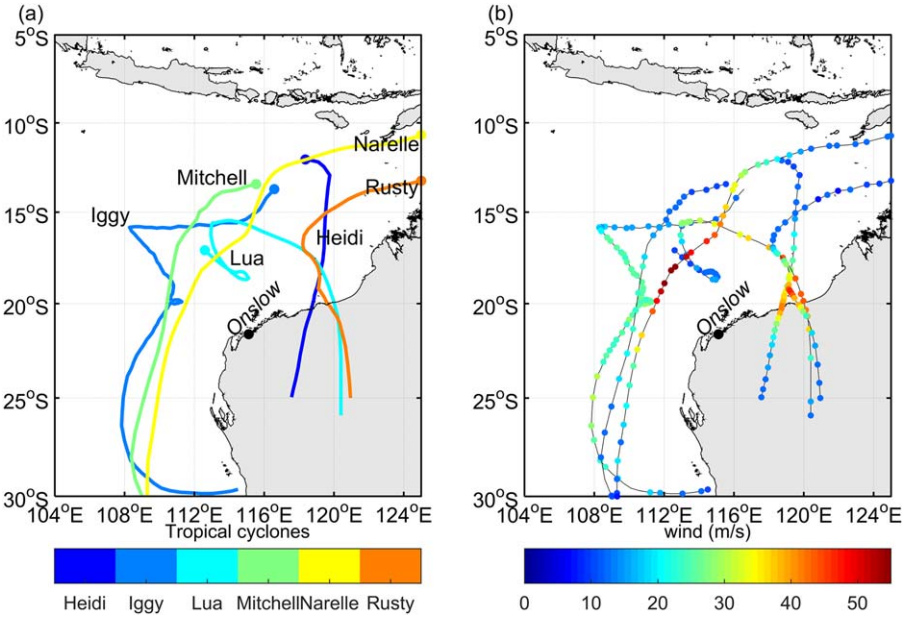

Figure 2. (a) Tracks and names of the tropical cyclones that passed within 1,000 km of Onslow between May 2011 and March 2013. The dots indicate the origin of the cyclone tracks. (b) The associated maximum wind speeds along the tracks (m s^{-1}).

radii ranging from 556 to 667 km (see supporting information Figure S1), and did not generate strong wind anomalies in Onslow.

The rainfall patterns during the TCs were variable both in terms of magnitude, duration, and phasing (Figure 3d). Of all the cyclones, Heidi generated the most rain over the Ashburton catchment area with 6 consecutive days exceeding 5 mm d^{-1} of rainfall, reaching up to 26 mm d^{-1}. During Lua, 1 day of strong rainfall (35 mm d^{-1}) occurred. The other TCs generated lower rainfall rates on land. The daily Ashburton River discharge appeared to be significantly correlated with the catchment area rainfall ($r = 0.46$, $p < 0.05$) with a lag of ~4 days. There was strong variability in the river discharge with a long lasting peak after Heidi and smaller discharge peaks after Iggy and Lua (Figure 3d).

4.2. Hydrodynamic Conditions

Over the shelf off Onslow (at sites JETTY, WEEKS, PAROO, and SPOILGC), the tidal currents reached up to 0.5 m s^{-1}, with the tidal ellipses roughly aligned along an east-west direction (directions ranging from 83° to 100°) . The subtidal flow over the shelf oscillated around an overall northwest-southwest direction (or east-west at JETTY) corresponding generally to the alongshore direction (i.e., the main variance axis aligned with the isobaths; Figure 4a). Those subtidal flows were homogeneous in direction throughout the water column at each location. There were high correlations for all locations between the alongshore current and the local alongshore wind (ERA-Interim) with r ranging from 0.61 to 0.83 ($p < 0.05$), except at the furthest offshore and deepest station PIL100 (Figure 4b). Subtidal currents during Iggy and Narelle reached ~0.3 m s^{-1} at the more coastal locations (JETTY, WEEKS, PAROO, and SPOILGC) and were among the strongest observed over the entire study period (Figure 4a). During those TCs, south-westward flowing subtidal currents were observed that lasted several days, peaking when the cyclones were directly off the coast (Figure 5). The peak of the flow occurred during the peak of southwestward alongshore winds induced by the TCs (Figure 4b and supporting information Figure S2). There was also a reversal of the subtidal flow to the northeast after the passage of the TCs, coinciding with a reversal of the alongshore wind. During Mitchell, similar subtidal current patterns were observed, although both the alongshore winds and currents were weaker. During Lua, a southwestward subtidal flow was followed by a northeastward flow after landfall and coincided with the reversal of the alongshore winds. Weaker subtidal currents with no clear correlation with the wind patterns were observed during Heidi and Rusty.

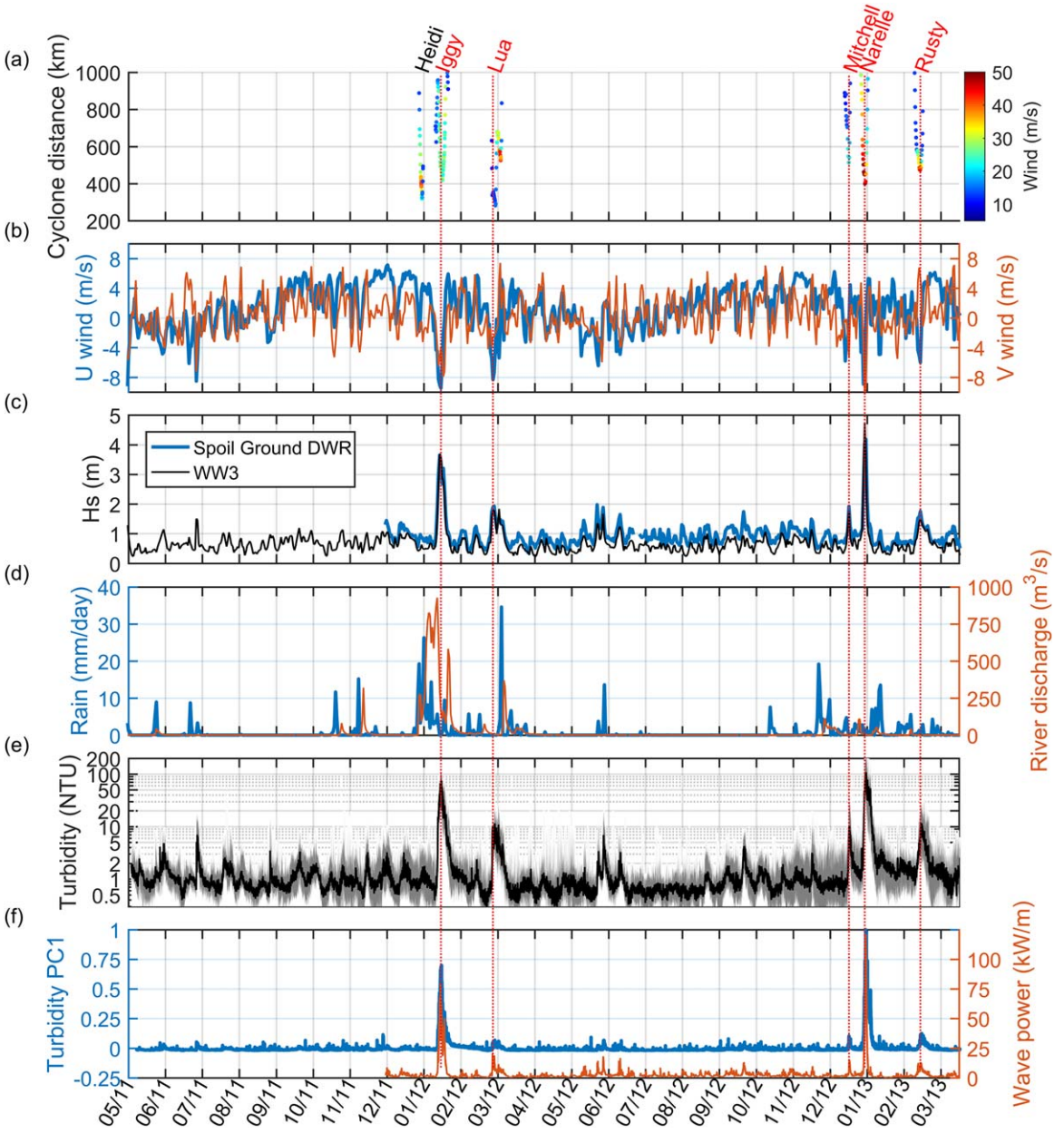

Figure 3. Meteorological conditions, wave forcing, and turbidity in the study area. (a) Distance (km) from Onslow to the various cyclones occurring in the area and maximum wind speed (m s^{-1}). (b) Eastward (U) and northward (V) daily winds (m s^{-1}) observed at Onslow. (c) Daily significant wave height (m) at SPOILG from the wave buoy (blue line) and from the CAWCR hindcast (black line). (d) Mean daily rainfall (mm d^{-1}) from gauges in the Ashburton River catchment area and river discharge (m^3 s^{-1}) at Nanutarra. (e) Hourly median turbidity (NTU) recorded by the 23 turbidity sensors (black line). The grey shading indicates the tenth and ninetieth percentile for all the sensors. (f) First principal component time series (PC1) of the turbidity sensor array (blue line) and wave power at Spoil Ground (red line).

Except for Heidi, all other TCs induced substantial increases in the significant wave heights over the shelf off Onslow (Figure 3c and supporting information Figure S3a). Iggy and Narelle induced the largest significant wave heights offshore at SPOILG, with H_s reaching 4.3 and 5.2 m, respectively, and a peak period (T_p) of ~12 s for both. Lua, Mitchell, and Rusty induced waves with H_s of 2.6, 2.2, and 2.0 m, and T_p of 10, 8, and 12 s, respectively. A few other wave events (with $H_s > 1.5$ m) of shorter duration were also observed independently of the presence of a TC. Those events were related to local wind peaks, generating higher frequency waves ($T_p < 8$ s). During TCs, wave attenuation was evident across the shelf, with smaller wave heights of 1.9 m observed at PAROO during Iggy and 2.2 m observed at JETTY during Narelle (supporting information Figures S3a, S4a, and S4c).

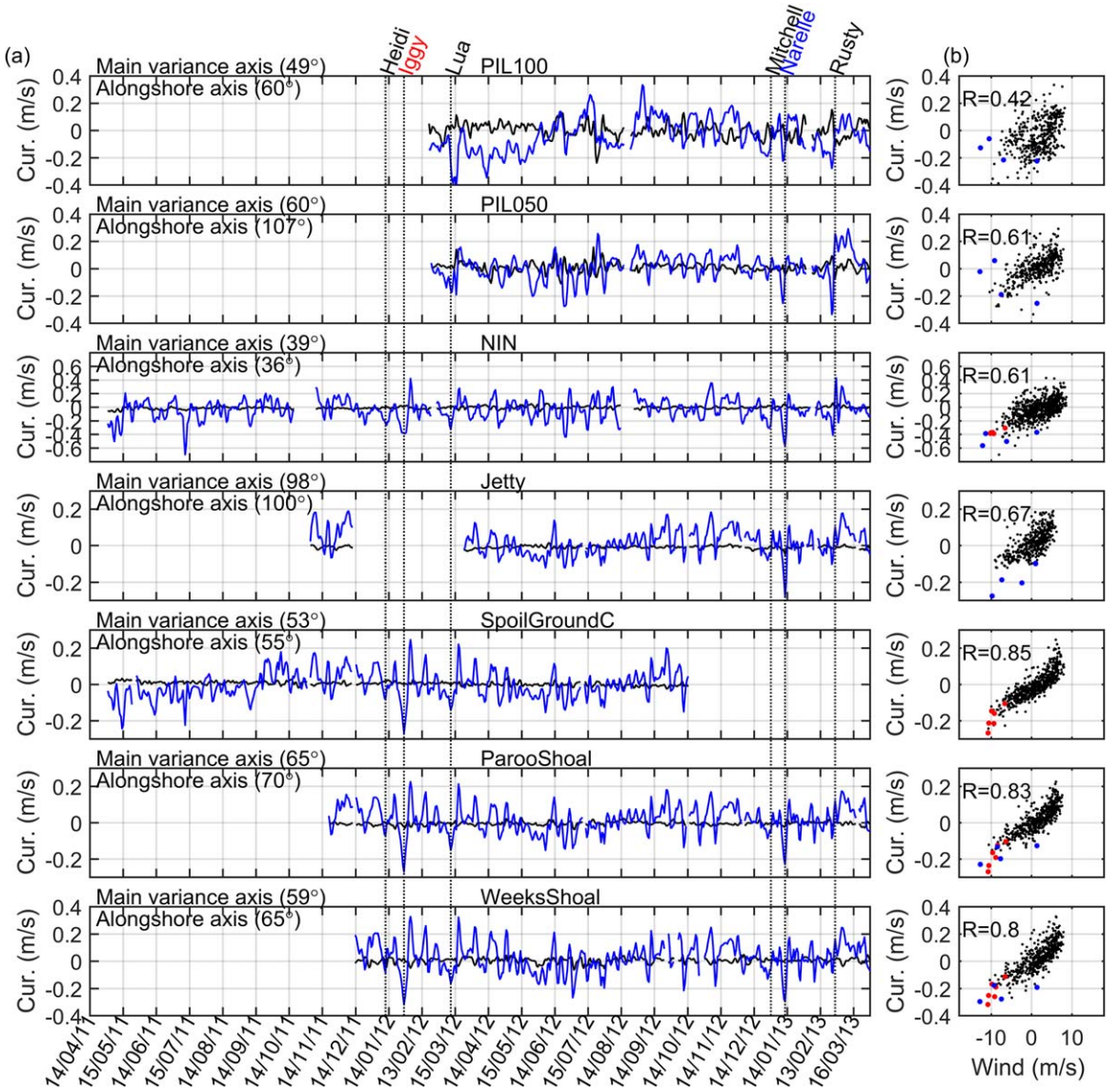

Figure 4. Daily subtidal depth-averaged currents. (a) Current velocities (m s^{-1}) along the major variance axis (blue) and minor variance axis (black) at various locations. (b) Current (m s^{-1}) velocities versus wind velocity (m s^{-1}) along the major variance axis of the current at the same locations. Blue dots correspond to the Iggy cyclone period (25 January 2012 to 31 January 2012) and red dots to Narelle (10 January 2013 to 14 January 2013). The directions of the major variance axis and the alongshore axis are indicated in each figure. Directions are given in degrees clockwise from north. Major axis is positive in the eastward direction and minor axis is positive in the northward direction.

4.3. Sediment Dynamics

4.3.1. In Situ Turbidity Variability

Over the shelf region off Onslow, the 23 turbidity sensors located between 7 and 12 m depth displayed very similar variability (Figure 3e). The main turbidity events (median turbidity exceeding 10 NTU) all occurred during TC events, with Iggy and Narelle inducing the highest turbidity values ranging between 21–192 and 36–250 NTU, respectively. The turbidity peaks during the other TCs (Lua, Mitchell, and Rusty) were ~1 order of magnitude lower. A tidal signal was present in the turbidity data, with a main energy peak at 12 h and a smaller one at 6 h (supporting information Figure S5). The amplitude of the tidally driven turbidity peaks were, however, 1–2 orders of magnitude smaller than the peaks observed during cyclone events (Figure 3e). The median of the hourly turbidity for all 23 sensors was best correlated with the observed H_s variability ($r = 0.71$, $p < 0.05$) and wave power ($r = 0.88$, $p < 0.05$) at SPOILG with a lag of 10 h. Strong correlations between the mean daily-averaged wave energy at SPOILG and the turbidity at all

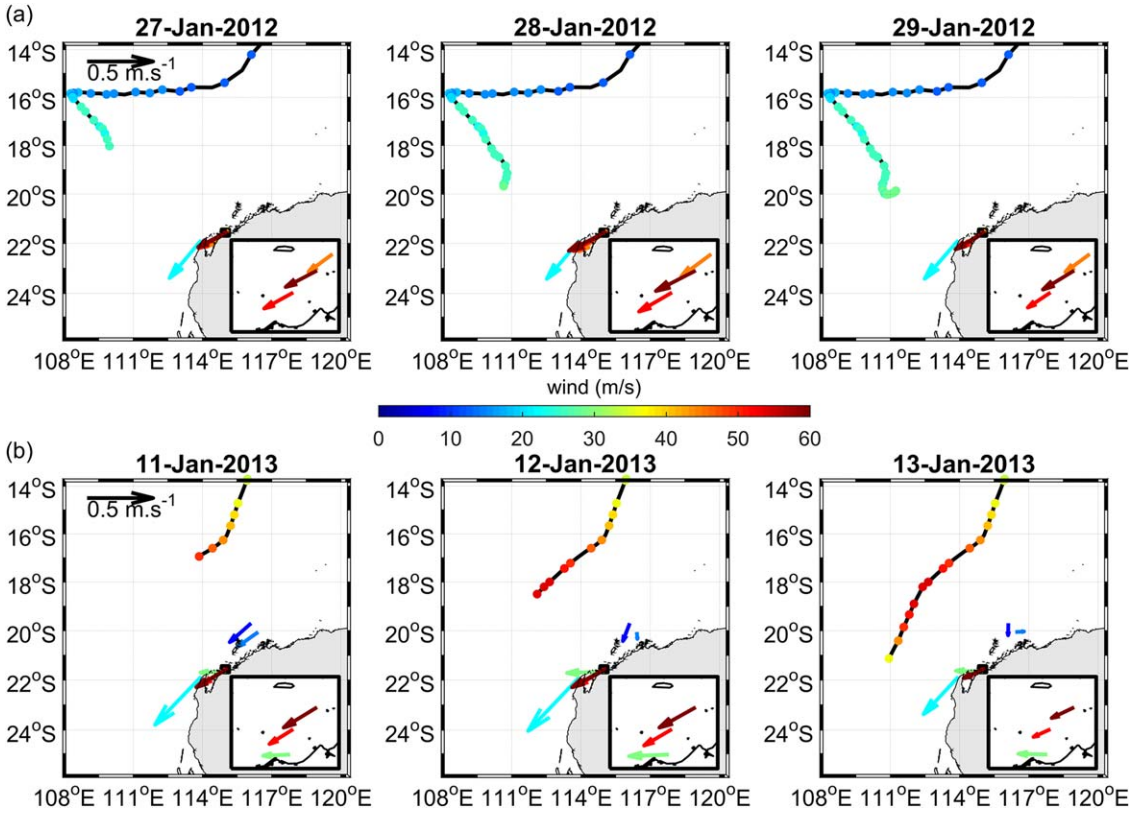

Figure 5. Daily subtidal currents during cyclone (a) Iggy and (b) Narelle at three successive dates during the peak current velocity events. Each current meter is represented by an arrow of different color. The box on the lower right corner of each figure is a zoom closer to Onslow. The cyclone track and the associated maximum wind speed (colorbar in m s^{-1}) is added (1 dot every 6 h).

locations were found, ranging from $r = 0.80$ to 0.93 ($p < 0.05$) for a lag ranging 0–1 day (Figure 6b and supporting information Figure S6b). The correlation between the median of the daily-averaged turbidity for all 23 sensors and the Ashburton River discharge reached 0.37 ($p < 0.05$) for a lag of 9 days. However, the correlations throughout the shelf were not homogeneous and reached a maximum just off the river mouth with $r = 0.66$ with a 10 days lag while ranging $r = 0.15$–0.59 elsewhere (Figure 6a and supporting information Figure S6a).

The Empirical Orthogonal Function (EOF) decomposition performed using the hourly turbidity data predicted a first mode that explained ~70% of the total variance. The subsequent modes were not significant, each representing less than 5% of the variance. The principal component time series (PC1) was mostly positive, and highlighted two main peaks during Iggy and Narelle, and smaller peaks during the other TCs (Figure 3f). The PC1 time series was best correlated with the wave power measured at SPOILG with a lag of 10 h ($r = 0.88$, $p < 0.05$). At the daily time scale, the PC1 and the Ashburton River discharge correlation reached $r = 0.45$ ($p < 0.05$) for a lag of 9 days. The spatial loading of this first mode (EOF1) generally highlighted higher values in the nearshore (Figure 7a). No significant correlations were found between EOF1 and the local site depth or the sediment composition (Figure 7b).

In order to provide insights into the vertical profile of turbidity, we converted the AWAC backscatter intensity data at PAROO into an approximate turbidity around the time of Iggy. The relative volume backscatter strength, BS_r (equation (2)), from the AWAC at 2 mab was strongly correlated with the common logarithm of the in situ turbidity ($r = 0.89$, $p < 0.05$; Figure 8a). The turbidity estimated from the AWAC (using $a = 0.82$ and $b = -55.3$ in equation (3)) was therefore in good agreement with the in situ turbidity near the seabed ($r = 0.80$, $p < 0.05$; Figure 8b). The turbidity estimated from the AWAC showed that suspended sediments were likely not confined near the seabed during Iggy and that turbidity may have increased both near the seabed and toward the surface (Figures 8c and 8d).

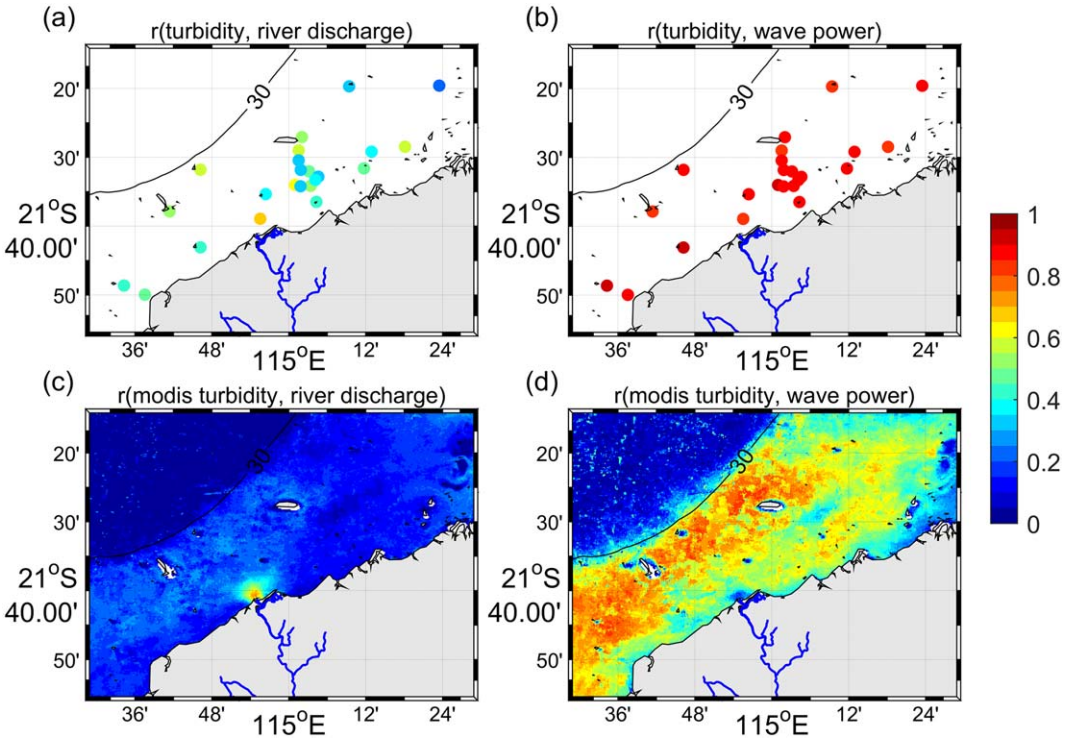

Figure 6. Best time-lagged correlation between the daily in situ turbidity and (a) the Ashburton River discharge and (b) the in situ wave power at Spoil Ground. Best time-lagged correlation between the weekly MODIS SSC (250 m resolution), and (c) the Ashburton River discharge and (d) the CAWCR wave power at SPOILG. The 30 m isobath is included for reference on all figures. Corresponding time-lags are provided in supporting information Figure S6.

4.3.2. Sedimentation Variability Inferred From the Sediment Traps

The highest sedimentation rates recorded by the sediment traps occurred within the period P2, which included Iggy, and during the period P10, which included Narelle and Mitchell (Figure 9a). There were also increased sedimentation rates observed during P3, which included Lua, and P11, which included Rusty. Although the absolute values of the sedimentation rates were somewhat variable throughout the shelf, the relative temporal variability (normalized by the maximum value) was homogeneous for all locations. Most of the trapped material was inorganic (mean = 90.5 ± 0.3%; SD = 3.2%; n = 109), giving confidence that during P10, when the inorganic content data were missing, the high total sedimentation rate also corresponded to high inorganic sedimentation (Figure 9a). There was a strong correlation between the mean turbidity over each sampling period at all locations and the sedimentation rate ($r = 0.80$; $p < 0.05$; n = 127 for the total rate, $r = 0.75$; $p < 0.05$; n = 115 for the inorganic rate).

Mud was the main size fraction of the trapped material, with silt and clay representing on average 27.1 ± 0.8% (SD = 9.3%; n = 151) and 52.3 ± 0.9% (SD = 10.7%; n = 151), respectively (Figure 9b). On average, there was an increase of the trapped sand fraction during the periods that included Iggy and Narelle (Figure 9b), although the response was variable across the different sites.

The surficial seabed samples contained only 9.3 ± 0.8% of mud on average (SD = 8.7%; n = 114; Figures 7b and 9c). The temporal variability of the seabed was also very variable among all the sites, but on average there seemed to be a slight increase of the coarser sediment fraction during the period that included Iggy.

4.3.3. Drivers of Sediment Dynamics Variability

We focused on the SALAD site to investigate the relationship between the local turbidity and hydrodynamic variability, given that it had the longest time series (~1.5 years) of turbidity and nearby current and wave data. Wave and current data were extrapolated from PAROO (~1.7 km away) assuming that the hydrodynamics remained similar between the two locations. The wave-induced BSS was one order of magnitude higher than the current-induced BSS during the various turbidity events at SALAD located at 11 m depth

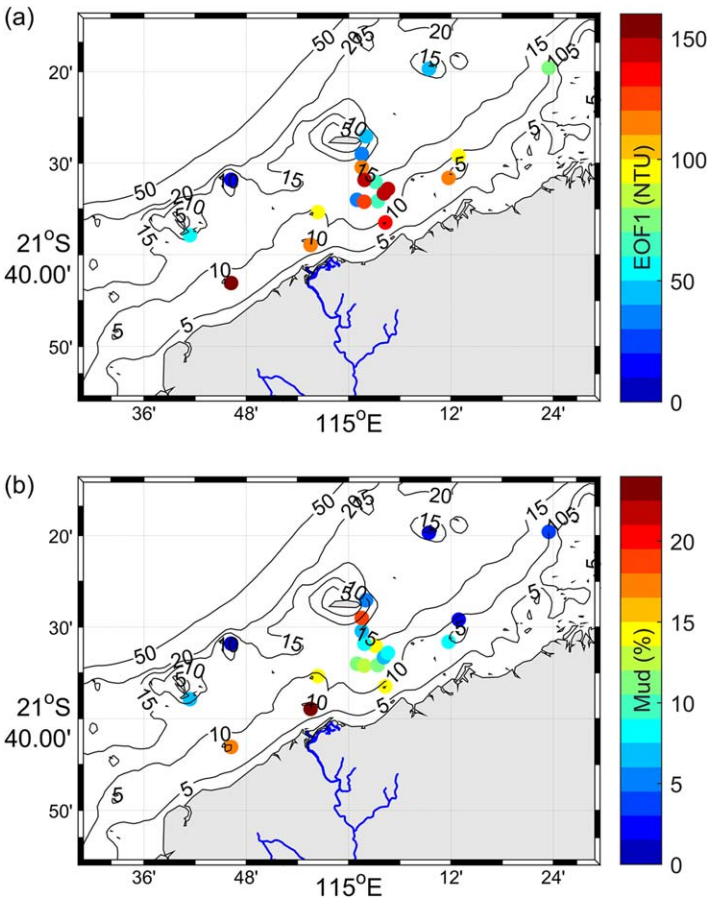

Figure 7. (a) Spatial loading of the first EOF (NTU) from the turbidity sensor array. The associated principal component time series is reported in Figure 2f. (b) Mean mud (silt and clay) fraction of the surficial sediment (%). Isobaths 5, 10, 15, 20, and 50 m are included in both figures.

(Figure 10a). There was a relatively good agreement between the local measurements of total BSS and turbidity with no lag (Figures 10b and 10c), with $r = 0.65$ ($p < 0.05$). This agreement was much better explained by the wave-induced BSS contribution ($r = 0.65$, $p < 0.05$) rather than the current-induced BSS ($r = 0.17$, $p < 0.05$). The correlation between the BSS with the turbidity further increased when considering the excess shear stress (max(BSS-BSS_c,0) where BSS_c is the critical shear stress), reaching a maximum at $r = 0.70$ ($p < 0.05$) for $BSS_c = 0.81$ N m^{-2} (obtained by least square fitting).

The cumulative turbidity flux (using hourly data) over the 17 month sampling period at SALAD was predominantly in a west-southwestward direction (Figure 10d). Furthermore, the turbidity fluxes occurring during Iggy and Narelle (blue and red lines in Figure 10d) were far higher than the fluxes integrated over the rest of the 17 month period (black lines on Figure 10d). The sediment flux was overall southwestward during the entire Iggy event, and during the peak of Narelle. During Narelle, higher turbidity remained after the peak of the BSS (Figure 10c), coinciding with a north-eastward reversal of the current (supporting information Figure S2). This led to a significant north-eastward sediment flux at the end of the Narelle event.

All of the above patterns observed at SALAD were very similar to what was observed at WEEKS (13 months long time series; supporting information Figure S7). The correlation between the excess shear stress and the turbidity reached a maximum at $r = 0.78$ ($p < 0.05$) for BSS_c=0.71 N m^{-2}. In addition, most of the southwestward residual sediment flux occurred during Iggy and Narelle.

Overall, the wave-induced BSS reached relatively high values over most of the shallow shelf (<50 m) during Iggy and Narelle (supporting information Figures S4b and S4d), and dominated the current-induced BSS at four shallow sites (i.e., at 15, 13.5, 10, and 8 m depths corresponding to SPOILGC, WEEKS, PAROO, and JETTY, respectively) across the shelf (Figure 10a and supporting information Figures S3b and S7a).

4.4. Spatial Variability in Sediment Dynamics Inferred From Remote Sensing

Based on the 14 year calibrated MODIS data set, the correlation between weekly SSC and the Ashburton River discharge reached a peak in the vicinity of the river mouth ($r = 0.76$, $p < 0.05$) but decreased rapidly away from the mouth ($r < 0.3$ further than 8 km off the mouth; Figure 6c). Although the strongest correlation between the two time series occurred with no lag at the river mouth, there seemed to generally be an ~1 week of lag with the river discharge over the rest of the shallow (<30 m) shelf (supporting information Figure S6c). The correlation between weekly MODIS SSC and the wave energy at SPOILG (predicted from the CAWCR wave hindcast) was relatively stronger, especially for locations of the shelf shallower than 30 m depth and reached a maximum of $r = 0.85$ ($p < 0.05$; Figure 6d). There was a good agreement between H_s at SPOILG from the wave buoy and from the CAWCR wave hindcast ($r = 0.86$, $p < 0.05$; Figure 3c) giving us confidence in using the longer time series from the wave hindcast (including further below).

The EOF decomposition performed using the weekly calibrated MODIS SSC data extracted a first mode of variability explaining 53.5% of the total variance at the scale of the surveyed (in situ data) area and ~30% at the scale of the broader North West Shelf (Figures 11a and 11b). The subsequent modes were not significant, each representing less than 10% of the total variance. The PC1 extracted for the two domains were very similar ($r = 0.95$, $p < 0.05$). Those PC1s compared well with the PC1 obtained from in situ data at the weekly scale, i.e., $r = 0.90$ ($p < 0.05$) and $r = 0.91$ ($p < 0.05$) for the smaller and the larger domains, respectively. This provides further confidence in using the MODIS SSC to assess the variability over longer time scales. The PC1s appeared to be well correlated with the weekly mean significant wave height at SPOILG

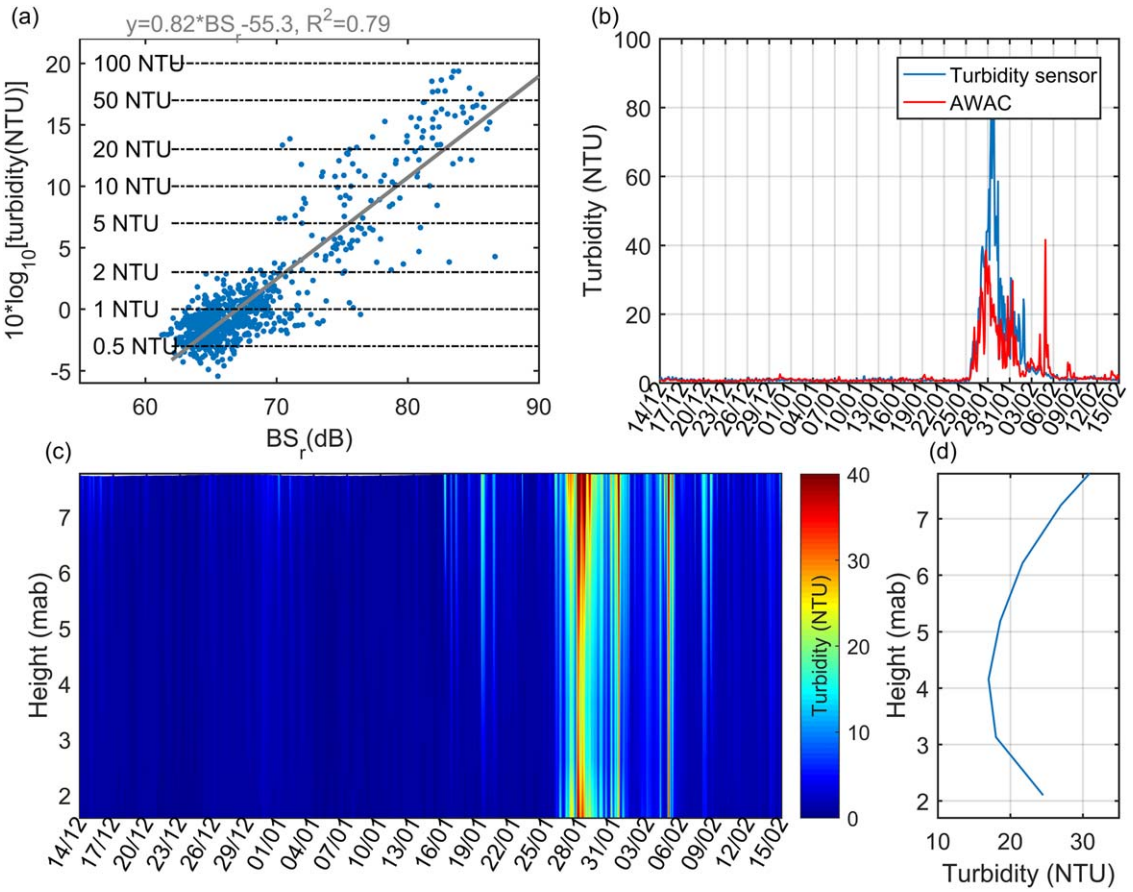

Figure 8. Turbidity from the AWAC located at PAROO around the TC Iggy event. (a) Scatterplot of the common logarithm of the turbidity (NTU) estimated by the turbidity sensor (at SALAD) versus the relative volume backscattering index BS_r (dB) given by the AWAC at 2 mab. (b) Time series of turbidity (NTU) from the turbidity sensor (blue) and from the AWAC (red) at 2 mab. (c) Turbidity (NTU) in the water column estimated by the AWAC. The *y* axis is the height above the seabed. (d) Mean vertical turbidity profile (NTU) from the AWAC during the peak of the event (27 January 2012 to 29 January 2012).

($r = 0.72$, $p < 0.05$ and $r = 0.71$, $p < 0.05$), and with the weekly mean wave energy ($r = 0.69$, $p < 0.05$ and $r = 0.73$, $p < 0.05$). Correlations between the PC1s and the rainfall were maximum with a 2 weeks lag ($r = 0.21$ and $r = 0.22$ for the smaller and the larger domains). Correlations between the Ashburton River discharge and the PC1 were maximum for the discharge leading by 1 week ($r = 0.21$ and $r = 0.23$ for the smaller and the larger domains). The spatial loading of the EOF1 indicated a gradual cross-shore decrease of the SSC, with values approaching 0 for depths greater than 30 m (Figure 11a).

The highest PC1 peaks occurred during Iggy and Narelle, but all of the peaks also coincided with other cyclone events (Figures 11b and 11c). The TCs that induced the highest turbidity increase during the period 06/2002 to 12/2015 (nine TCs with PC1 > 0.27) generally had higher wave heights and stronger southwestward winds (Figures 11b–11e and 12a). Apart from TC Quang, which propagated cross-shore, all the other TCs that generated increased turbidity (PC1 > 0.27) were propagating alongshore (Figure 12b). For the period 01/1979 to 05/2002, prior to the MODIS data used in this study, nine cyclones induced wave height greater than 3 m at SPOILG, including TC Vance which induced the highest H_s (5.8 m) of the whole time series. These TCs generally propagated into an alongshore direction and induced substantial southwestward winds in Onslow (Figure 12).

5. Discussion

By combining 2 years of in situ data (consisting of turbidity sensors, sediment traps, current profilers/meters, and wave buoys) and a 14 year weekly satellite SSC product we showed that cyclones overwhelmingly dominate the natural sediment dynamics over the southern part of the Australian North West Shelf.

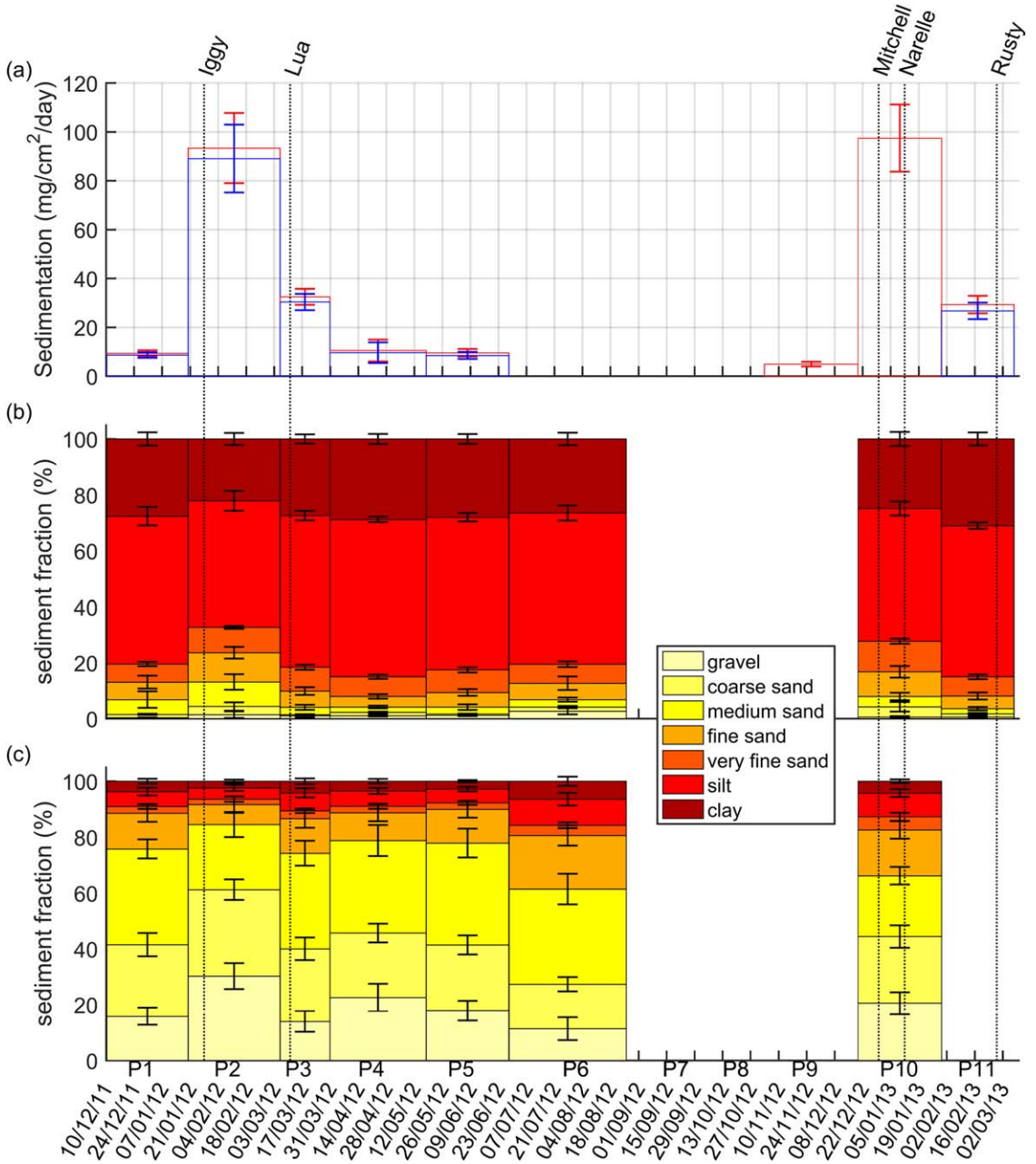

Figure 9. Mean sediment trap data for the 20 stations for the different sampling periods (P1–P11). The whiskers correspond to the standard error (SE). (a) Mean sedimentation rates (mg cm^2 d^{-1}). Blue bars correspond to the inorganic sedimentation rate, while red bars correspond to the total sedimentation. (b) Mean sediment composition of the trapped material. (c) Mean sediment composition of the surficial seabed.

5.1. Cyclone-Induced Sediment Resuspension Over the Shelf

Local extreme wave conditions induced by the TCs were the primary driver of turbidity variations across the NWS study region across a range of temporal scales and spatial scales. The sediment trap data suggested that the increase of turbidity observed near the seabed during the TCs was mostly composed of fine sediments that are likely to be most readily stirred up into the water column. Both the turbidity estimated by the AWAC and the surface SSCs estimated from the satellite data suggest that the elevated SSCs during the TCs impacted the entire water column from seabed to surface (Figure 8d). The strong relationship between local wave conditions (or more specifically the wave-induced BSS) and turbidity suggested that local sediment resuspension by waves was the main process driving the SSC increase during TC events at the shelf scale, particularly in depths shallower than 30 m.

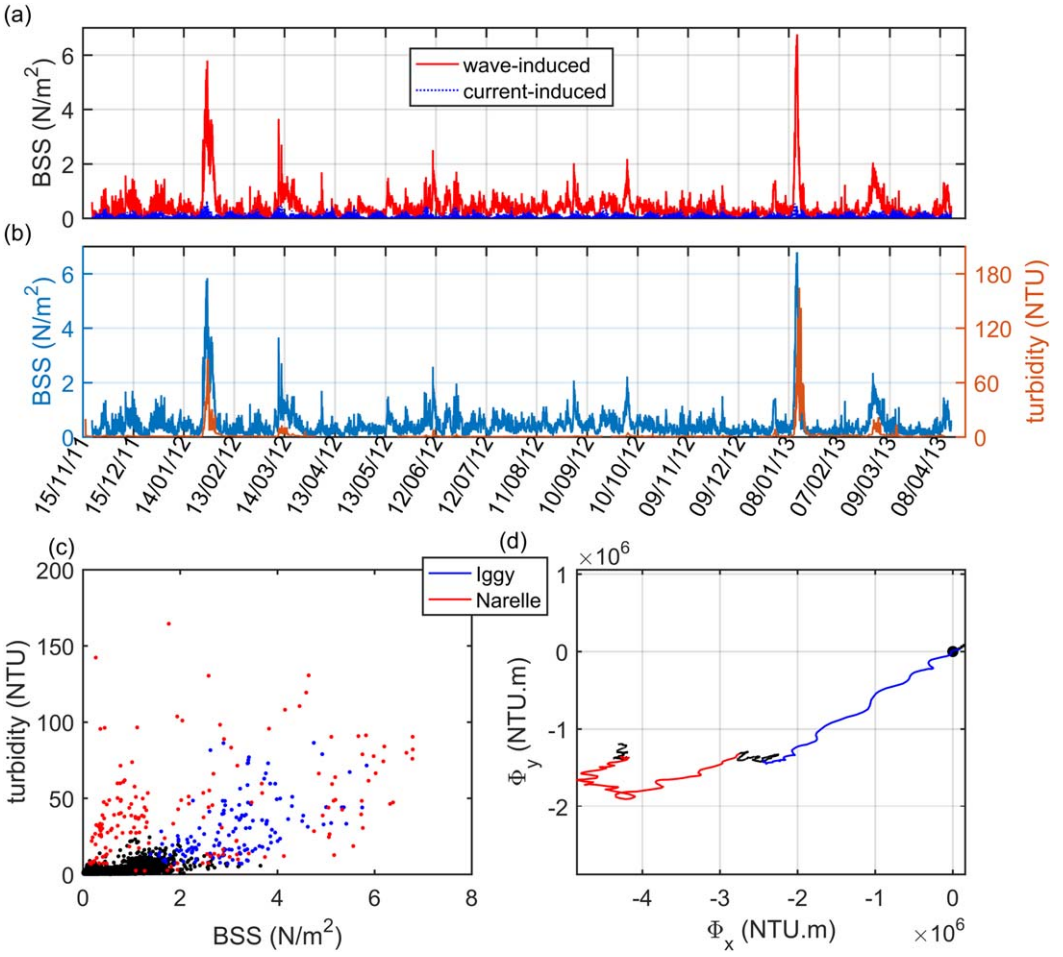

Figure 10. Hourly bottom shear stress (BSS), turbidity, and horizontal sediment fluxes at SALAD (wave and current data are from PAROO). (a) Wave-induced (red) and current-induced (blue) bottom shear stress (N m^{-2}). (b) Total bottom shear stress (N m^{-2}) and turbidity (NTU). (c) Turbidity versus total bottom shear stress. (d) Cumulative horizontal turbidity fluxes (NTU m). The starting point ($\Phi_x=0, \Phi_y=0$) is represented by the black dot; the integration period coincides with the time period in Figures 10a and 10b. In (c) and (d), the blue lines and dots correspond to the Iggy cyclone period (26 January 2012 to 31 January 2012) and the red ones to Narelle (11 January 2013 to 17 January 2013).

There was a clear decoupling between the seabed sediment properties (mostly composed of coarse material, but still comprising muds around 10%), and the suspended material, mostly composed of fine material (Figures 9a and 9b), suggesting that selective resuspension occurred. An increase of the fraction of coarser sediment (sand to gravel) was observed in the traps during the most energetic TCs (Iggy and Narelle). This is consistent with the hypothesis of local resuspension, with increased BSS during the TC events reaching the critical erosion threshold of larger grain sizes.

Assuming that local resuspension dominated over sediment advection, our analysis estimated a critical BSS of 0.71 and 0.81 N m^{-2} for fine sediment resuspension at two different locations where median seabed sediment diameter was 720 and 1,650 μm (which according to a Shields curve with these diameters, would predict a critical shear stress of 0.35 and 1.02 N m^{-2}, respectively, for these sediments). The critical shear stresses estimated in our study are thus rather large for fine sediments, which suggests that bed-armoring or hiding/sheltering by the coarser sediment fraction (Wu et al., 2000) may have been occurring.

Although turbidity peaks were observed at tidal frequencies in the data set, these turbidity variations were 1–2 orders of magnitude smaller than those driven by TCs (Figure 3 and supporting information Figure S5), despite the tides being relatively large over parts of the study area (e.g., ∼3–4 m in the study region). This confirms that TCs are the predominant driver of sediment resuspension along this part of the NWS.

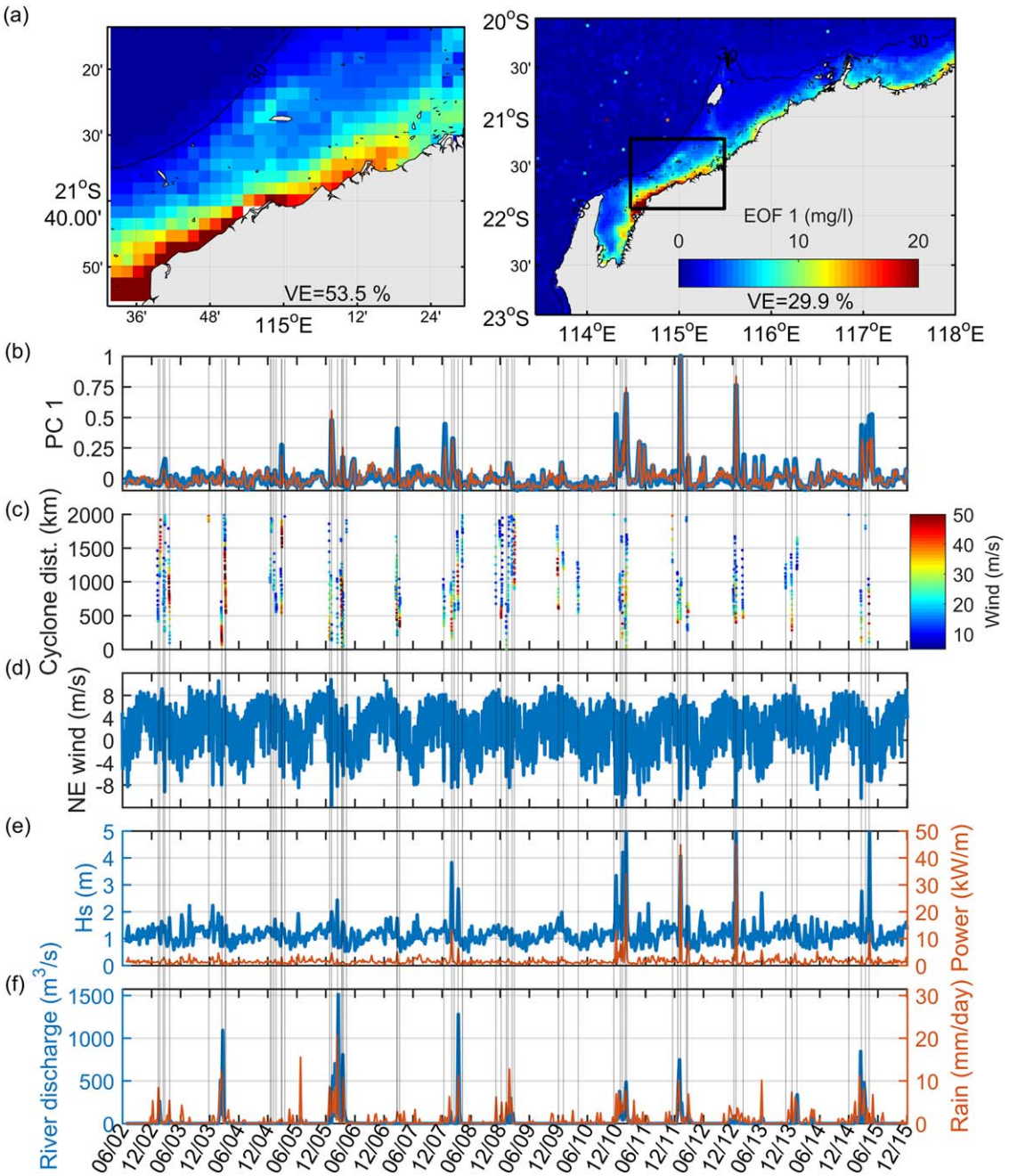

Figure 11. (a) First EOF (mg L^{-1}) of the MODIS SSC data set (4 km resolution) for two different domains. The variance explained (VE) by this mode is indicated. Isobaths 30 m is added. (b) First principal component time series of the MODIS SSC data set for two different domains (smaller domain in blue and larger domain in red). (c) Distance (km) from Onslow to the various cyclones occurring in the area and maximum wind speed (m s^{-1}). (d) Daily north-eastward wind (rotated winds; negative values indicate south-westward winds) at Onslow from ERA. (e) Weekly maximum significant wave height (m) and mean wave power (kW m^{-1}) at Spoil Ground from the CAWCR wave hindcast. (f) Mean weekly rainfall (mm d^{-1}) over the Ashburton River catchment area and river discharge (m^3 s^{-1}) at Nanutarra.

5.2. Cyclone-Induced Sediment Fluxes

Over the 2 year period when in situ data were available, the horizontal sediment fluxes were dominated by just two locally intense cyclones: Iggy and Narelle (Figure 10d). Not only did these cyclones produce the highest waves, and hence the highest resuspension rates and SSC over the shelf, but they also induced sustained wind-driven southwestward flows reaching up to 0.3 m s^{-1} over a large part of the southern NWS (Figure 5), concomitant with the SSC peak (supporting information Figure S2). These two events dominated the total southwestward sediment flux over the 2 year period; outside of these short-lived pulses (i.e., under

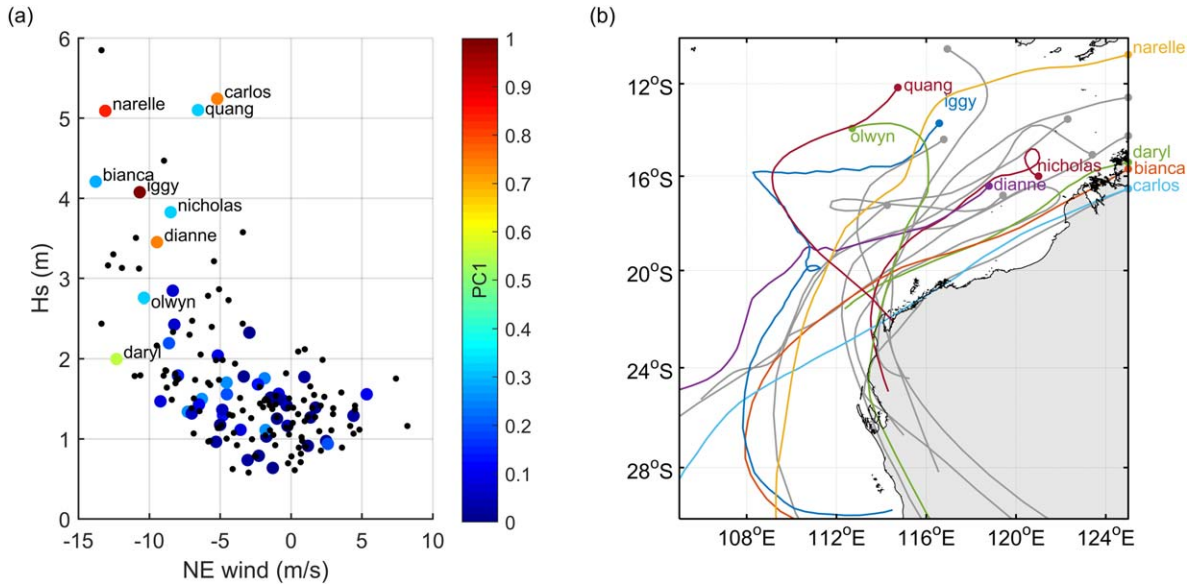

Figure 12. (a) Daily maximum significant wave height (m) at site SPOILG from the CAWCR wave hindcast versus minimum north-eastward wind (rotated winds; negative values indicate south-westward winds) at Onslow from ERA for all TC events spanning 01/1979 to 12/2015. Color dots are for the TCs during the period of the MODIS SSC data (06/2002 to 12/2015), with color indicating the maximum PC1 value occurring during each event. Cyclone names are given when PC1 $>$ 0.27. (b) Track of the TCs with PC1 $>$ 0.27 (colored lines) during the MODIS SSC period and with $H_s > 3$ m for the rest of the time period (grey lines). The dots indicate the origin of the cyclone tracks.

normal background conditions), these fluxes were relatively small (Figure 10d). Although a limited number of modeling studies lacking field observations have suggested TCs to be the primary driver of resuspension before tides along the southern part of the NWS (Harris, 1995; Harris et al., 2000; Porter-Smith et al., 2004), the present study provides direct (observational) evidence that TCs are the predominant drivers of sediment transport throughout the shelf.

The barotropic response of the circulation of the NWS to cyclone-induced winds has previously been shown to generate strong southwestward currents based on alongshore tracks of typical cyclones (Fandry & Steedman, 1994; Hearn & Holloway, 1990). Those modeling studies confirm that the circulation patterns observed during TCs in our study (Figure 5) have a shelf scale extent. This response has been shown to induce rapid southwestward transport of larvae during a TC (McKinnon et al., 2003). We also observed that the subtidal currents over the shelf were mostly alongshore during the TCs, which were particularly strong during Iggy and Narelle due to the intense local wind conditions that were generated (Figure 4).

Quasi-geostrophic continental shelf waves can also be triggered by TCs over the NWS (Eliot & Pattiaratchi, 2010). For most of the cyclones we focused on in this study, the wind and current velocity fluctuations appeared phase locked (supporting information Figure S2). The observed wind-driven response can therefore be described as a "forced" continental shelf wave, consisting of a locally generated surge travelling with the synoptic wind forcing (Eliot & Pattiaratchi, 2010; LeBlond & Mysak, 1978). There was no obvious appearance of "free" or freely propagating continental shelf waves, except potentially during Heidi and Rusty when local winds and currents were more decoupled.

Observed sediment concentrations could also potentially be impacted by advection of remotely resuspended sediment. Combined with cyclone-induced mixing (Toffoli et al., 2012) likely being able to maintain sediments in suspension over longer time periods, the subtidal flows could indeed explain some mismatch observed between the local resuspension capacity and the turbidity along the trailing edge of the turbidity peak, notably during Narelle (Figure 10c and supporting information Figure S2).

5.3. Responses to Different Cyclone Characteristics

By extending our observations over a longer 14 year period using calibrated MODIS SSC data, our results suggest that the strong alongshore propagating TCs are more likely to generate stronger waves and higher turbidity levels than the cross-shore propagating TCs (Figure 12). Furthermore, alongshore propagating TCs

generate strong southwestward winds due to the clockwise wind rotation and orientation of the coastline, in turn inducing sustained wind-driven southwestward flows. We therefore suggest that alongshore propagating TCs, which have both high erosion and transport potential, make a dominant contribution to the sediment pathways over the shelf. Furthermore, using data from a longer (37 year) wind and wave hindcast, our results indicate that among the 186 cyclones approaching the study region (within 1,500 km of Onslow), at least 16 of them had a strong potential for simultaneous sediment resuspension and transport, due to the high waves (>3 m) and strong sustained southwestward winds (Figure 12).

5.4. Cyclone-Induced Riverine Sediment Discharge

TCs can induce extreme rainfall over land, and therefore provide large pulses of sediment by rivers into the coastal zone. The main river system in the southern NWS study region is the Ashburton River. The spatial patterns exhibited by the correlation maps between river discharge and turbidity suggested that the riverine sediment discharge is a main driver of turbidity variability only over a relatively small area local to the river mouth (Figures 6a and 6c). This does not mean that the river would have no influence beyond close proximity to the river mouth; for example, sediment concentrations would be diluted as the river plume propagates into deeper waters, which would lower its surface signature. Instead, it implies that when considering the vast scale of the entire shelf, resuspension and advection overwhelm any signal from the river except near its mouth. The increase of turbidity close to the surface observed by the AWAC during Iggy could potentially be seen as a direct impact from the river discharge (Figure 8). This could however also be due to an artefact of the backscattering inversion method due to the injection of bubbles deeper down the water column when wind increases (Jourdin et al., 2014). In any case, rivers are most likely a significant source of new fine sediments over the shelf and could contribute to maintaining available muds within the surficial sediment cover and therefore provide a means to enhance turbidity variability during subsequent TC events.

No in situ data were available to track the sediment river discharge and therefore only remote sensing data could be used in this study. Owing to the uncertainties introduced by satellite estimations of SSC in coastal and riverine waters (e.g., the difficulty in disentangling water-leaving reflectance induced by chlorophyll, suspended sediment and colored dissolved organic matter; Gholizadeh et al., 2016), further in situ based studies would be necessary to rigorously assess the role of river discharge in the overall sediment budget of the NWS.

6. Conclusions

While the hydrodynamic response to the intense forcing by TCs on the NWS has been widely studied, detailed assessments of how TCs drive its shelf sediment dynamics have been lacking. Through analysis of in situ data, remote sensing data and long-term wave and wind hindcast data, the results revealed how sediment dynamics vary across multiple spatial and temporal scales. Our study highlighted the role of wave-induced sediment resuspension in modulating the turbidity over the shelf. TCs were the main driver of SSC variability and horizontal sediment fluxes over the southern part of the NWS. This alongshore sediment pathway induced by TCs is comparable to the Australian Great Barrier Reef alongshore northward sediment transport resulting from TCs, which has been shaping the shelf for the last 5,000 years (Larcombe & Carter, 2004). Although we can expect this cyclone-induced alongshore sediment transport to also be acting over the northern part of the NWS, further investigations are needed to determine the residual sediment pathway over that part of the shelf due to the northward gradual increase of tide-induced resuspension over the shelf (Porter-Smith et al., 2004). In the future, the use of a state-of-the-art couple air/sea/wave/sediment transport model (Ricchi et al., 2017) could be beneficial to get a more comprehensive picture of the sediment dynamics at the shelf scale under a range of TC conditions, including assessing the role of the cyclone-induced river discharge in contributing to the overall turbidity and providing fine sediments to the seabed.

Acknowledgments

The authors thank the two reviewers for their valuable comments on the manuscript. This project was partially funded by the Western Australian Marine Science Institution (WAMSI) as part of the WAMSI Dredging Science Node and made possible through investment from Woodside Energy, Chevron Australia, BHP Billiton as environmental offsets and by coinvestment from the WAMSI Joint Venture partners. Additional support was provided by the Australian Research Council Centre of Excellence for Coral Reef Studies. Data used in this study were partially provided by Chevron Australia as part of the Wheatstone project. The commercial investors and data providers had no role in the data analysis, data interpretation, and the decision to publish or in the preparation of the manuscript. The portion of the data related to the Wheatstone project can be requested for noncommercial use from WAMSI (info@wamsi.org.au) by establishing a data agreement. The processed and calibrated MODIS SSC data can be accessed through the National Computational Infrastructure data server available at http://remote-sensing.nci.org.au/. Additional mooring data were obtained from Australia's Integrated Marine Observing System (IMOS) available at https://portal.aodn.org.au/. Wave hindcast data were obtained from the Centre for Australian Weather and Climate Research available from http://doi.org/10.4225/08/523168703DCC5.

References

Bahmanpour, M. H., Pattiaratchi, C., Wijeratne, E. M. S., Steinberg, C., & D'Adamo, N. (2016). Multi-year observation of Holloway Current along the shelf edge of North Western Australia. *Journal of Coastal Research*, *75*(sp1), 517–521.

Bridge, T. C. L., Done, T. J., Beaman, R. J., Friedman, A., Williams, S. B., Pizarro, O., & Webster, J. M. (2011). Topography, substratum and benthic macrofaunal relationships on a tropical mesophotic shelf margin, central Great Barrier Reef, Australia. *Coral Reefs*, *30*(1), 143–153. https://doi.org/10.1007/s00338-010-0677-3

Chevron. (2011). *Final Environmental Impact Statement/response to submissions on the Environmental Review and Management Programme for the Proposed Wheatstone Project* (Technical Report, 337 pp.). Perth, WA, Australia: Chevron Australia Pty Limited.

Chevron. (2016). *Wheatstone Project Dredging and Dredge Spoil Placement Environmental Monitoring and Management Plan* (Tech. Rep. WS0-0000-HES-RPT-CVX-000–00086-000, Revision 4). Perth, WA, Australia: Chevron Australia Pty Limited.
Condie, S., Andrewartha, J., Mansbridge, J., & Waring, J. (2006). *Modelling circulation and connectivity on Australia's North West Shelf* (Technical Report, 62 pp.). Canberra, Australia: CSIRO.
Condie, S., & Andrewartha, J. R. (2008). Circulation and connectivity on the Australian North West Shelf. *Continental Shelf Research*, *28*(14), 1724–1739.
Condie, S., Herzfeld, M., Margvelashvili, N., & Andrewartha, J. R. (2009). Modeling the physical and biogeochemical response of a marine shelf system to a tropical cyclone. *Geophysical Research Letters*, *36*, L22603. https://doi.org/10.1029/2009GL039563
D'Adamo, N., Fandry, C., Buchan, S., & Domingues, C. (2009). Northern sources of the Leeuwin Current and the "Holloway Current" on the North West Shelf. *Journal of the Royal Society of Western Australia*, *92*(2), 53–66.
Dail, M. B., Corbett, D. R., & Walsh, J. P. (2007). Assessing the importance of tropical cyclones on continental margin sedimentation in the Mississippi delta region. *Continental Shelf Research*, *27*(14), 1857–1874.
Davidson, F. J. M., & Holloway, P. E. (2003). A study of tropical cyclone influence on the generation of internal tides. *Journal of Geophysical Research*, *108*(C3), 3082.
Dee, D. P., Uppala, S. M., Simmons, A. J., Berrisford, P., Poli, P., Kobayashi, S., . . . Vitart, F. (2011). The ERA-Interim reanalysis: Configuration and performance of the data assimilation system. *Quarterly Journal of the Royal Meteorological Society*, *137*(656), 553–597. https://doi.org/10.1002/qj.828
Dorji, P., Fearns, P., & Broomhall, M. (2016). A semi-analytic model for estimating total suspended sediment concentration in turbid coastal waters of northern Western Australia using MODIS-Aqua 250 m data. *Remote Sensing*, *8*(7), 556.
Downing, A., Thorne, P. D., & Vincent, C. E. (1995). Backscattering from a suspension in the near field of a piston transducer. *The Journal of the Acoustical Society of America*, *97*(3), 1614–1620.
Drost, E. J. F., Lowe, R. J., Ivey, G. N., Jones, N. L., & Péquignet, C. A. (2017). The effects of tropical cyclone characteristics on the surface wave fields in Australia's North West region. *Continental Shelf Research*, *139*, 35–53.
Dufois, F., Verney, R., Le Hir, P., Dumas, F., & Charmasson, S. (2014). Impact of winter storms on sediment erosion in the Rhone River prodelta and fate of sediment in the Gulf of Lions (North Western Mediterranean Sea). *Continental Shelf Research*, *72*, 57–72.
Durrant, T., Greenslade, D., Hemer, M., & Trenham, C. (2014). *A global wave hindcast focussed on the Central and South Pacific* (Tech. Rep. 070, 45 pp.). Melbourne, Australia: CAWCR.
Eliot, M., & Pattiaratchi, C. (2010). Remote forcing of water levels by tropical cyclones in southwest Australia. *Continental Shelf Research*, *30*(14), 1549–1561. https://doi.org/10.1016/j.csr.2010.06.002
Fandry, C. B., & Steedman, R. K. (1994). Modelling the dynamics of the transient, barotropic response of continental shelf waters to tropical cyclones. *Continental Shelf Research*, *14*(15), 1723–1750.
Fearns, P., Dorji, P., Broomhall, M., Branson, P., & Mortimer, N. (2017a). *Plume characterisation—Laboratory studies. Final report of Theme 2.3 Project 3.2.2 of the Western Australian Marine Science Institution (WAMSI) dredging science node* (Technical Report). Crawley, WA, Australia: Western Australian Marine Science Institution.
Fearns, P., Dorji, P., Broomhall, M., Chedzey, H., Symonds, G., Shimizu, K., . . . Sun, C. (2017b). *Plume characterisation. Final report of Theme 2.3 Project 3.2 of the Western Australian Marine Science Institution (WAMSI) dredging science node* (Technical Report). Crawley, WA, Australia: Western Australian Marine Science Institution.
Fisher, R., Stark, C., Ridd, P., & Jones, R. (2015). Spatial patterns in water quality changes during dredging in tropical environments. *PLoS ONE*, *10*(12), e0143309.
Galewsky, J., Stark, C. P., Dadson, S., Wu, C. C., Sobel, A. H., & Horng, M. J. (2006). Tropical cyclone triggering of sediment discharge in Taiwan. *Journal of Geophysical Research*, *111*, F03014. https://doi.org/10.1029/2005JF000428
Gholizadeh, M. H., Melesse, A. M., & Reddi, L. (2016). A comprehensive review on water quality parameters estimation using remote sensing techniques. *Sensors*, *16*(8), 1298.
Gingele, F. X., De Deckker, P., & Hillenbrand, C.-D. (2001). Clay mineral distribution in surface sediments between Indonesia and NW Australia—Source and transport by ocean currents. *Marine Geology*, *179*(3), 135–146. https://doi.org/10.1016/S0025-3227(01)00194-3
Godin, G. (1972). *The analysis of tides* (264 pp.). Toronto, Canada: University of Toronto Press.
Haig, T. (2009). *The Pilbara coast water study. Hydrogeological record series* (Tech. Rep. HG 34). Perth, WA, Australia: Western Australia Department of Water.
Hamilton, L. J. (1997). Methods to obtain representative surface wave spectra, illustrated for two ports of north-western Australia. *Marine and Freshwater Research*, *48*(1), 43–57.
Harris, P. T. (1995). Marine geology and sedimentology of the Australian continental shelf. In *The State of the Marine Environment Report for Australia, Technical Annex 1* (pp. 11–23). Canberra, Australia: Department of the Environment, Sport and Territories.
Harris, P. T., Smith, R., Anderson, O., Coleman, R., & Greenslade, D. (2000). *GEOMAT—Modelling of continental shelf sediment mobility in support of Australia's regional marine planning process* (Geoscience Australia Record 41). Canberra, Australia: Australian Geological Survey Organisation.
Hearn, C. J., & Holloway, P. E. (1990). A three-dimensional barotropic model of the response of the Australian North West Shelf to tropical cyclones. *Journal of Physical Oceanography*, *20*(1), 60–80.
Hemer, M. A., Zieger, S., Durrant, T., O'Grady, J., Hoeke, R. K., McInnes, K. L., & Rosebrock, U. (2016). A revised assessment of Australia's national wave energy resource. *Renewable Energy*, *111*(A), 85–107. https://doi.org/10.1016/j.renene.2016.08.039
Holloway, P. E. (1983). Tides on the Australian north-west shelf. *Marine and Freshwater Research*, *34*(1), 213–230. https://doi.org/10.1071/MF9830213
Holloway, P. E. (1995). Leeuwin Current observations on the Australian North West Shelf, May–June 1993. *Deep Sea Research, Part I: Oceanographic Research Papers*, *42*(3), 285–305. https://doi.org/10.1016/0967-0637(95)00004-P
James, N. P., Bone, Y., Kyser, T. K., Dix, G. R., & Collins, L. B. (2004). The importance of changing oceanography in controlling late Quaternary carbonate sedimentation on a high-energy, tropical, oceanic ramp: North-western Australia. *Sedimentology*, *51*(6), 1179–1205. https://doi.org/10.1111/j.1365-3091.2004.00666.x
Jones, H. A. (1973). *Marine geology of the Northwest Australian Shelf* (Technical Report, 136 pp.). Canberra, Australia: Australian Government Publishing Service, Bureau of Mineral Resources.
Jones, R., Fisher, R., Stark, C., & Ridd, P. (2015). Temporal patterns in seawater quality from dredging in tropical environments. *PLoS ONE*, *10*(10), e0137112.
Jourdin, F., Tessier, C., Hir, P. L., Verney, R., Lunven, M., Loyer, S., . . . Lepesqueur, J. (2014). Dual-frequency ADCPs measuring turbidity. *Geo-Marine Letters*, *34*(4), 381–397.

Larcombe, P., & Carter, R. M. (2004). Cyclone pumping, sediment partitioning and the development of the Great Barrier Reef shelf system: A review. *Quaternary Science Reviews*, *23*(1), 107–135.
LeBlond, P. H., & Mysak, L. A. (1978). *Waves in the ocean, Elsevier Oceanography Series* (602 pp.). New York, NY: Elsevier.
Legendre, P., & Legendre, L. F. J. (2012). *Numerical ecology*. Amsterdam, the Netherlands: Elsevier.
Liu, J. T., Wang, Y.-H., Yang, R. J., Hsu, R. T., Kao, S.-J., Lin, H.-L., & Kuo, F. H. C. C. (2012). Cyclone-induced hyperpycnal turbidity currents in a submarine canyon. *Journal of Geophysical Research*, *117*, C04033. https://doi.org/10.1029/2011JC007630
Longley, I. M., Buessenschuett, C., Clydsdale, L., Cubitt, C. J., Davis, R. C., Johnson, M. K., . . . Spry, T. B. (2002). The North West Shelf of Australia—A Woodside perspective. Paper presented at the Proceedings of the Petroleum Exploration Society of Australia symposium, the sedimentary basins of Western Australia 3, Perth, Australia.
Lough, J. M. (1998). Coastal climate of northwest Australia and comparisons with the Great Barrier Reef: 1960 to 1992. *Coral Reefs*, *17*(4), 351–367.
Madsen, J. D., Chambers, P. A., James, W. F., Koch, E. W., & Westlake, D. F. (2001). The interaction between water movement, sediment dynamics and submersed macrophytes. *Hydrobiologia*, *444*(1), 71–84. https://doi.org/10.1023/A:1017520800568
Margvelashvili, N. Y., Andrewartha, J. R., Condie, S. A., Herzfeld, M. G., Parslow, J. S., Sakov, P. V., & Waring, J. R. (2006). *Modelling suspended sediment transport on Australia's North West Shelf* (Tech. Rep. 7, 43 pp.). Canberra, Australia: CSIRO.
McKinnon, A. D., Meekan, M. G., Carleton, J. H., Furnas, M. J., Duggan, S., & Skirving, W. (2003). Rapid changes in shelf waters and pelagic communities on the southern Northwest Shelf, Australia, following a tropical cyclone. *Continental Shelf Research*, *23*(1), 93–111. https://doi.org/10.1016/S0278-4343(02)00148-6
Porter-Smith, R., Harris, P. T., Andersen, O. B., Coleman, R., Greenslade, D., & Jenkins, C. J. (2004). Classification of the Australian continental shelf based on predicted sediment threshold exceedance from tidal currents and swell waves. *Marine Geology*, *211*(1–2), 1–20. https://doi.org/10.1016/j.margeo.2004.05.031
Rayson, M. D., Ivey, G. N., Jones, N. L., Lowe, R. J., Wake, G. W., & McConochie, J. D. (2015). Near-inertial ocean response to tropical cyclone forcing on the Australian North-West Shelf. *Journal of Geophysical Research: Oceans*, *120*, 7722–7751. https://doi.org/10.1002/2015JC010868
Rayson, M. D., Ivey, G. N., Jones, N. L., Meuleners, M. J., & Wake, G. W. (2011). Internal tide dynamics in a topographically complex region: Browse Basin, Australian North West Shelf. *Journal of Geophysical Research*, *116*, C01016. https://doi.org/10.1029/2009JC005881
Ricchi, A., Mario, M. M., Barbariol, F., Benetazzo, A., Bergamasco, A., Bonaldo, D., . . . Carniel, S. (2017). Sensitivity of a Mediterranean tropical-like cyclone to different model configurations and coupling strategies. *Atmosphere*, *8*(5), 92.
Ridgway, K. R., & Godfrey, J. S. (2015). The source of the Leeuwin Current seasonality. *Journal of Geophysical Research: Oceans*, *120*, 6843–6864. https://doi.org/10.1002/2015JC011049
Semeniuk, V. (1993). The Pilbara coast: A riverine coastal plain in a tropical arid setting, northwestern Australia. *Sedimentary Geology*, *83*(3), 235–256. https://doi.org/10.1016/0037-0738(93)90015-W
Sherman, C., Schmidt, W., Appeldoorn, R., Hutchinson, Y., Ruiz, H., Nemeth, M., . . . Xu, H. (2016). Sediment dynamics and their potential influence on insular-slope mesophotic coral ecosystems. *Continental Shelf Research*, *129*, 1–9. https://doi.org/10.1016/j.csr.2016.09.012
Soulsby, R. (1997). *Dynamics of marine sands: A manual for practical applications*. London, UK: Thomas Telford.
Tessier, C. (2006). *Caractérisation et dynamique des turbidités en zone côtière: L'exemple de la région marine Bretagne Sud* (PhD thesis). Talence, France: Université de Bordeaux 1.
Tessier, C., Le Hir, P., Lurton, X., & Castaing, P. (2008). Estimation of suspended sediment concentration from backscatter intensity of Acoustic Doppler Current Profiler. *Comptes Rendus Geoscience*, *340*(1), 57–67.
Tian, T., Merico, A., Su, J., Staneva, J., Wiltshire, K., & Wirtz, K. (2009). Importance of resuspended sediment dynamics for the phytoplankton spring bloom in a coastal marine ecosystem. *Journal of Sea Research*, *62*(4), 214–228. https://doi.org/10.1016/j.seares.2009.04.001
Toffoli, A., McConochie, J., Ghantous, M., Loffredo, L., & Babanin, A. V. C. C. J. (2012). The effect of wave-induced turbulence on the ocean mixed layer during tropical cyclones: Field observations on the Australian North-West Shelf. *Journal of Geophysical Research*, *117*, C00J24. https://doi.org/10.1029/2011JC007780
Van Gastel, P., Ivey, G. N., Meuleners, M. J., Antenucci, J. P., & Fringer, O. (2009). The variability of the large-amplitude internal wave field on the Australian North West Shelf. *Continental Shelf Research*, *29*(11), 1373–1383. https://doi.org/10.1016/j.csr.2009.02.006
WAMSI. (2015). *The Blueprint for Marine Science 2050. Research directions to enhance industry competitiveness and government effectiveness in the marine environment off Western Australia* (Technical Report). Perth, Australia: Western Australian Marine Science Institution.
Webster, I. (1985). Wind-driven circulation on the North West Shelf of Australia. *Journal of Physical Oceanography*, *15*(11), 1357–1368.
Wilson, B. (2013). *The biogeography of the Australian North West Shelf: Environmental change and life's response* (640 pp.). San Diego, CA: Elsevier.
Wolanski, E., Fabricius, K. E., Cooper, T. F., & Humphrey, C. (2008). Wet season fine sediment dynamics on the inner shelf of the Great Barrier Reef. *Estuarine, Coastal and Shelf Science*, *77*(4), 755–762. https://doi.org/10.1016/j.ecss.2007.10.014
Wu, W., Wang, S. S. Y., & Jia, Y. (2000). Nonuniform sediment transport in alluvial rivers. *Journal of Hydraulic Research*, *38*(6), 427–434.
Xu, J., Lowe, R. J., Ivey, G. N., Jones, N. L., & Brinkman, R. (2015). Observations of the shelf circulation dynamics along Ningaloo Reef, Western Australia during the austral spring and summer. *Continental Shelf Research*, *95*, 54–73.